BOSS DR12 full-shape cosmology: ΛCDM constraints from the large-scale galaxy power spectrum and bispectrum monopole

Oliver H. E. Philcox[1,2,*] and Mikhail M. Ivanov[2,†]

[1]*Department of Astrophysical Sciences, Princeton University, Princeton, New Jersey 08540, USA*
[2]*School of Natural Sciences, Institute for Advanced Study, 1 Einstein Drive, Princeton, New Jersey 08540, USA*

(Received 13 December 2021; accepted 30 January 2022; published 11 February 2022)

We present a full ΛCDM analysis of the BOSS DR12 dataset, including information from the power spectrum multipoles, the real-space power spectrum, the reconstructed power spectrum and the bispectrum monopole. This is the first analysis to feature a complete treatment of the galaxy bispectrum, including a consistent theoretical model and without large-scale cuts. Unlike previous works, the statistics are measured using window-free estimators: this greatly reduces computational costs by removing the need to window-convolve the theory model. Our pipeline is tested using a suite of high-resolution mocks and shown to be robust and precise, with systematic errors far below the statistical thresholds. Inclusion of the bispectrum yields consistent parameter constraints and shrinks the σ_8 posterior by 13% to reach $<5\%$ precision; less conservative analysis choices would reduce the error bars further. Our constraints are broadly consistent with *Planck*: in particular, we find $H_0 = 69.6^{+1.1}_{-1.3}$ kms^{-1} Mpc^{-1}, $\sigma_8 = 0.692^{+0.035}_{-0.041}$ and $n_s = 0.870^{+0.067}_{-0.064}$, including a BBN prior on the baryon density. When n_s is set by *Planck*, we find $H_0 = 68.31^{+0.83}_{-0.86}$ kms^{-1} Mpc^{-1} and $\sigma_8 = 0.722^{+0.032}_{-0.036}$. Our S_8 posterior, 0.751 ± 0.039, is consistent with weak lensing studies, but lower than *Planck*. Constraints on the higher-order bias parameters are significantly strengthened from the inclusion of the bispectrum, and we find no evidence for deviation from the dark matter halo bias relations. These results represent the most complete full-shape analysis of BOSS DR12 to-date, and the corresponding spectra will enable a variety of beyond-ΛCDM analyses, probing phenomena such as the neutrino mass and primordial non-Gaussianity.

DOI: 10.1103/PhysRevD.105.043517

I. INTRODUCTION

In the standard paradigm, the distribution of matter in the early Universe obeys Gaussian statistics, and can thus be fully described by its power spectrum [e.g., [1,2]]. As the Universe evolves, gravitational evolution induces non-Gaussianity [e.g., [3]], affording a complex matter distribution, with information distributed over a broad range of statistics. Why, then, do so few analyses of late-time cosmological data [e.g., [4–7]], use observables beyond the power spectrum?

Since the early 2000s, spectroscopic galaxy surveys have been played a role in the development of the cosmological model through their ability to measure the Universe's growth rate and expansion history using the baryon acoustic oscillation (BAO) feature [e.g., [6–12]]. This provides a "standard ruler" whose physical scale can be predicted by theory, and whose angular scale can be measured observationally, giving information on the distance-redshift relation, and hence the Hubble parameter $H(z)$ and angular diameter distance $D_A(z)$. Due to gravitational evolution, BAO effects are present not only in the power spectrum but also higher-order statistics: usually, one accounts for this by performing BAO reconstruction [e.g., [13–15]] to shift the corresponding information back into the two-point function [16] (though see [17] for a BAO measurement using the bispectrum).

While the BAO is certainly an important part of the galaxy power spectrum, it is by no means the only feature. Recent developments in theoretical modeling, in particular, the development of the effective field theory of large scale structure (EFTofLSS), have allowed a number of groups to fit the full power spectrum shape (rather than just the oscillatory component), and thus place constraints on the cosmological parameters directly [18–21]. This is akin to the analysis of CMB data, and enhances the cosmological utility of current and future surveys. The approach has further been combined with BAO information from reconstructed spectra [22], and used to place constraints on nonstandard cosmological models, such as nonflat universes [23], early dark energy [24,25], massive relics [26] and ultralight axions [27]. Furthermore, it can be used to

*ohep2@cantab.ac.uk
†ivanov@ias.edu

extract quantities orthogonal to that found in traditional scaling analyses, such as the scale of matter-radiation equality [28], which provides a powerful test of the cosmological model.

The natural question is whether such analyses can be extended to higher-order statistics, such as the galaxy bispectrum. Indeed, this is a natural place to look, since the bispectrum appears at the same order in perturbation theory as the oft-used one-loop power spectrum. However, modeling the bispectrum is difficult. Although a wealth of previous studies have discussed its theoretical form, both for matter and galaxies [29–33,33–46], it is only recently that we have obtained a theory model that is capable of predicting the full galaxy bispectrum shape in redshift-space to the precision required for current and future surveys [47].

Application of bispectrum models to true data is hampered by the effects of survey geometry. In particular, this leads to a triple convolution of the true bispectrum with the survey window function; an effect which is costly to replicate in practice, especially if one must sample the model many thousands of times. Previous works [6,7,17,31,48–50] have avoided this problem by making certain assumptions, most commonly, that the action of the window can be reproduced by instead window-convolving the *power spectrum* (noting that the tree-level bispectrum depends on two power spectra). However, this assumption is unwarranted. First, it introduces four copies of the survey mask rather than three (two per power spectrum), and second, it does not account for the full geometric structure of the statistic. This has led to previous studies removing triangle configurations most strongly affected by the window (those involving large-scale (soft) k-modes), which are also those in which signatures of new physics (such as primordial non-Gaussianity) can be most easily seen. If we wish to perform a full bispectrum study, such assumptions must be avoided. One route is to project the bispectrum onto a new basis [51,52]; this allows the window functions to be straightforwardly applied, though comes at the cost of having to similarly project the theoretical model.

In this work, we make use of the power spectrum and bispectrum estimators proposed in [53,54]. Analogous to methods discussed in the late 1990s [e.g., [55–58]], these estimate the true (unwindowed) power spectrum and bispectrum directly, and thus obviate the need to window-convolve the theory model. A naïve implementation of such approaches is computationally prohibitive, in particular, due to the need to compute the covariance matrix between each pixel in the dataset, and the requirement to estimate a large-dimensional Fisher matrix, which acts to deconvolve the statistic. However, the approach can be made efficient using modern computational techniques. Given these measurements, we perform a full analysis of the large-scale power spectrum and bispectrum of the BOSS DR12 galaxy data [59], utilizing the latest theoretical models derived within the EFTofLSS, in particular those of the one-loop power spectrum [60], reconstructed power spectrum [22], and tree-level bispectrum [47,61].[1] This stretches beyond previous studies in three key ways: (1) the window function is self-consistently treated, requiring no large-scale modes to be excluded, (2) we include a full treatment of all physical effects, (3) we measure cosmological parameters directly, instead of heuristic scaling parameters (such as BAO distortion parameters and amplitude ratios). In the current work, we consider only constraints on ΛCDM physics; however, an important extension is to measure nonstandard parameters, in particular those of primordial non-Gaussianity (see [66] for a recent forecast). This will be discussed in future work.

The structure of this paper is as follows. Our main cosmological results are summarized in Fig. 1 and in Table I, with the power spectrum and bispectrum measurements shown in Fig. 2, and bias parameter constraints depicted in Fig. 10. We begin by describing the observational data in Sec. II, before discussing our power spectrum and bispectrum estimators in Sec. III. Section IV presents our perturbative model for the power spectrum and bispectrum (including extension to the real-space power spectrum, to allow for a larger k-range), as well as the likelihood used in our analyses. The methodology is tested in Sec. V, before we present the main results of our analysis in Sec. VI. We conclude with a summary and discuss future work in Sec. VII, with additional parameter constraints given in the Appendix. Our measurements and likelihoods are made publicly available online.[2]

II. DATASETS

The primary dataset of this work is the twelfth data-release (DR12) of the Baryon Oscillation Spectroscopic Survey (BOSS) [59], part of SDSS-III [67]. In total, the survey contains over a million galaxies, observed in two disjoint regions of the sky; the Northern and Southern galactic caps (NGC and SGC). We divide the survey into two contiguous redshift slices, hereafter 'z1' and 'z3', encompassing $0.2 < z < 0.5$ and $0.5 < z < 0.75$ respectively (with effective redshifts 0.38 and 0.61), giving a total of four chunks. This is the decomposition used in previous power spectrum analyses [e.g., [12,18,19]] though we note that it mixes galaxies from the CMASS and LOWZ samples, which will have implications for the effective bias parameters. In full, we use the publicly available "CMASSLOWZTOT" galaxy samples,[3] filtered by redshift, and define the survey window function using the

[1] An important aspect of our theoretical model is an efficient IR resummation scheme for the redshift-space power spectrum and bispectrum, such as that derived within the time-sliced perturbation theory approach [62–65].

[2] See GitHub.com/oliverphilcox/BOSS-Without-Windows and GitHub.com/oliverphilcox/full_shape_likelihoods.

[3] Available at data.sdss.org/sas/dr12/boss/lss.

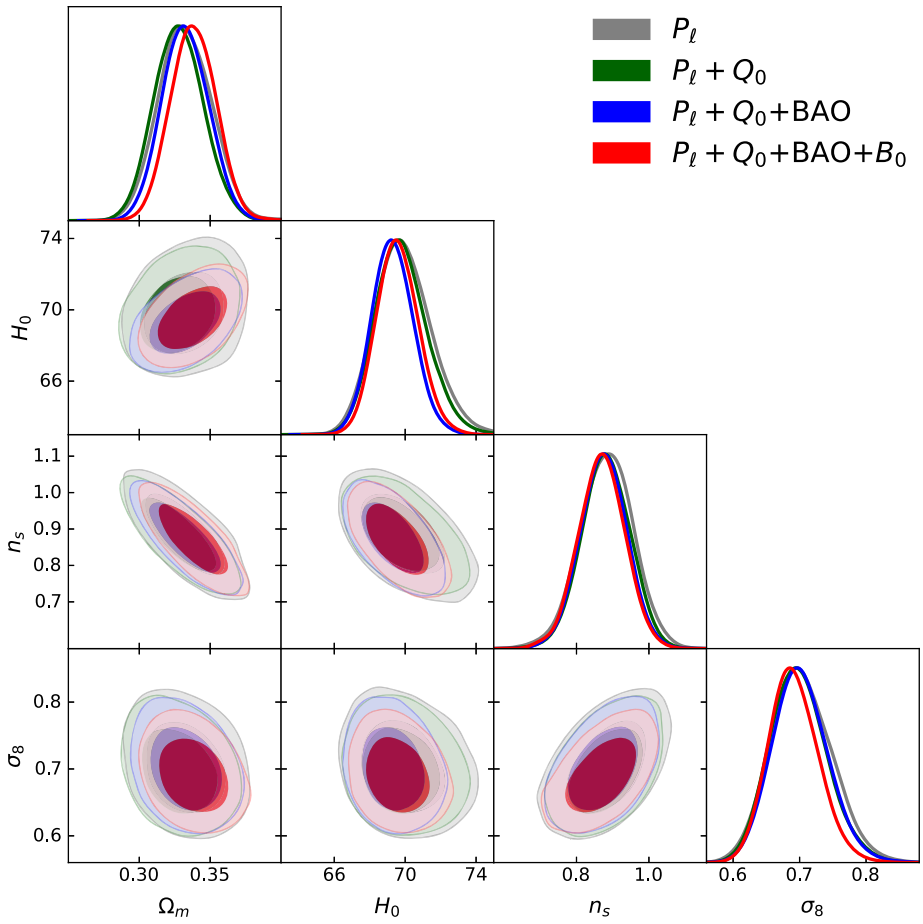

FIG. 1. ΛCDM parameter constraints from the full BOSS DR12 galaxy dataset, using the following combinations of statistics, as well as a BBN prior on the baryon density: the (window-free) redshift-space power spectrum P_ℓ up to $k_{\rm max} = 0.2h$ Mpc^{-1} (gray), the above plus the real-space power spectrum proxy Q_0 (green) up to $k_{\rm max} = 0.4h$ Mpc^{-1} (green), the above plus BAO parameters from the postreconstructed power spectrum (blue), the above plus the bispectrum monopole B_0 up to $k_{\rm max} = 0.08h$ Mpc^{-1} (red). The bispectrum is the main new feature of this work, and leads to a tightening of σ_8 by ≈10%, with the modest improvement linked to our conservative analysis choices. The σ_8 posteriors are $\approx 1\sigma$ larger than those found in some former analyses; this is due to an error in the public power spectra, as discussed in Sec. VI A 2. Table I gives the associated marginalized posteriors for each analysis shown above.

public MANGLE mask (required for the estimators of Sec. III) as well as a set of random particles, with fifty times the galaxy density. The latter are additionally used to define the overdensity field. As in previous works, we use the following galaxy weights:

$$w_{\rm tot} = (w_{\rm rf} + w_{\rm fc} - 1) w_{\rm sys}, \tag{1}$$

encoding redshift-failure, fiber-collision and systematic effects respectively [12].[4]

To construct a Gaussian likelihood for our dataset, we require a covariance matrix, which is here obtained using a (publicly available) suite of 2048 "MultiDark-Patchy" mock catalogs (hereafter PATCHY) [68,69]. Each is generated using an approximate gravity solver, and calibrated to an N-body simulation, providing an approximate form for the galaxy survey. These utilize a similar survey mask to the BOSS data and are generated using the cosmology $\{\Omega_m = 0.307115, \sigma_8 = 0.8288, h = 0.6777, \sum m_\nu = 0\}$. A weight is associated with each particle:

$$w_{\rm tot} = w_{\rm veto} w_{\rm fc}, \tag{2}$$

involving a veto mask and a fiber collision term. We use a separate random catalog for the PATCHY simulations.

Due to their approximate nature, the PATCHY mocks are not sufficiently accurate to test our analysis pipeline. Instead, we make use of the 84 NSERIES mock catalogs[5]

[4]Note that optimality weights [such as the Feldman-Kaiser-Peacock (FKP) weight] are naturally included in the estimators of Sec. III.

[5]Available at www.ub.edu/bispectrum/page11.html.

TABLE I. Mean and 68% confidence intervals for cosmological parameters from the main analysis of this work (matching Fig. 1). A full summary of these analyses can be found in Table III, with the analogous results from an analysis with *Planck* priors on n_s given in Table IV. H_0 posteriors are given in km s^{-1} Mpc^{-1} units.

Dataset	Ω_m	H_0	n_s	σ_8
$P_\ell(k)$	$0.332^{+0.019}_{-0.020}$	$69.9^{+1.5}_{-1.7}$	$0.883^{+0.076}_{-0.072}$	$0.704^{+0.044}_{-0.049}$
$P_\ell(k) + Q_0(k)$	$0.328^{+0.017}_{-0.019}$	$69.8^{+1.3}_{-1.6}$	$0.880^{+0.068}_{-0.068}$	$0.699^{+0.040}_{-0.046}$
$P_\ell(k) + Q_0(k) + \mathrm{BAO}$	$0.333^{+0.016}_{-0.018}$	$69.3^{+1.1}_{-1.3}$	$0.874^{+0.067}_{-0.064}$	$0.701^{+0.040}_{-0.045}$
$P_\ell(k) + Q_0(k) + \mathrm{BAO} + B_0$	$0.338^{+0.016}_{-0.017}$	$69.6^{+1.1}_{-1.3}$	$0.870^{+0.067}_{-0.064}$	$0.692^{+0.035}_{-0.041}$

[10]; these are computed from full N-body simulations (though are not fully independent) using similar selection functions and halo occupation distribution to the BOSS data, as well as full treatment of fiber collisions. The NSERIES mocks use the true cosmology $\{\Omega_m = 0.286, \sigma_8 = 0.82, n_s = 0.97, h = 0.7, \sum m_\nu = 0\}$. Unlike the

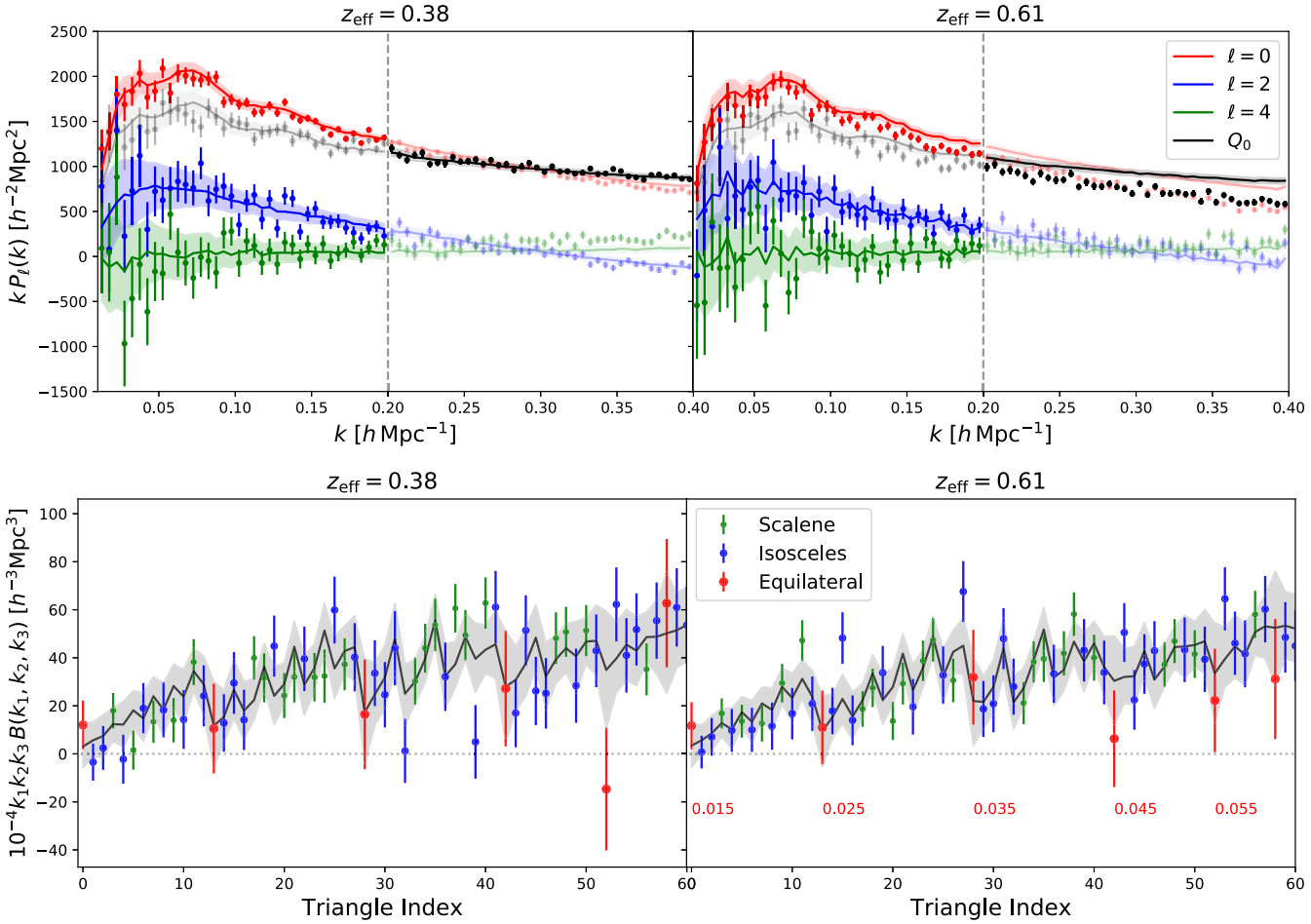

FIG. 2. Measured power spectra (top) and bispectra (bottom) from the BOSS dataset (points) and 2048 PATCHY mocks (lines and shaded regions) for two redshift bins z1 (left) and z3 (right). For the power spectra, we show measurements from the monopole, quadrupole, and hexadecapole, in red, blue, and green respectively, as well as the Q_0 statistic, $Q_0(k) \equiv P_0(k) - (1/2)P_2(k) + (3/8)P_4(k)$, which is a proxy for the real-space power spectrum. The vertical line disambiguates regions fit with the full power spectrum multipoles (left) and those with Q_0; the other regions (shown in faint lines) are not used in the analysis. For bispectra, we plot all triangle bins included in the analysis with $k < 0.08h$ Mpc^{-1}, noting that the observed structure arises from the bin ordering. These are ordered by triangle side, with scalene, isosceles, and equilateral triangles shown in green, blue, and red respectively. The red numbers in the right panel give the value of k for each equilateral bin. For clarity, we have combined estimates from the NGC and SGC regions (weighting by their sky fractions, with $f_{\rm NGC} \approx 0.7$); these are treated as separate samples in the main analysis of this work.

BOSS data, galaxies are not split into "z1" and "z3" chunks; rather, the simulations include only the CMASS NGC sample, spanning $0.43 < z < 0.7$ (with effective redshift $z_{\rm eff} = 0.56$). This has a different geometry to the BOSS data, but due to its large cumulative volume, provides a sensitive test of our methodology, in particular that of systematic and geometric effects. The dataset contains completeness weights and has an associated random catalog. Since the NSERIES data uses a different survey geometry, it requires a different covariance matrix; here this is generated using 2048 PATCHY simulations with the NSERIES window function (hereafter dubbed "PATCHY-NSERIES"). In total, we have four different random catalogs—BOSS, PATCHY, NSERIES and PATCHY-NSERIES—each of which are separately treated using the estimators of Sec. III. In all cases, data are converted to Cartesian coordinates assuming the fiducial cosmology: $\{\Omega_{m,\rm fid} = 0.31, h_{\rm fid} = 0.676\}$, which is used to calibrate the geometric distortion parameters (i.e., Alcock-Paczynski parameters) of Sec. IV.

Finally, we include a prior on the physical baryon density of $\omega_b = 0.02268 \pm 0.0038$, from big bang nucleosynthesis (BBN) considerations [70–72]; this has a similar width to that from *Planck* [73]. While we keep the tilt, n_s, free in our baseline analyses, we additionally consider a scenario in which it is fixed to the *Planck* best-fit ($n_s = 0.9649$), to allow for comparison with other full-shape analyses.

III. ESTIMATORS

Previous works have constrained cosmology from the power spectrum and bispectrum by measuring the statistics using simple FKP-like estimators [e.g., [6,12,74–76]]. Since the true galaxy distribution is modulated by a survey mask, the spectra are convolved with a nontrivial function of this mask, which must be replicated in the theoretical model. While this can be simply implemented using FFTs for the power spectrum, it is more difficult for the bispectrum, since one must perform a six-dimensional convolution integral. This has led to previous studies excising regions of the spectrum most affected by the window, leading to a loss of information. Here, we adopt a different approach, instead measuring the unwindowed power spectrum and bispectrum directly from the observational data.

To do this, we use the quadratic and cubic estimators discussed in [53,54]. These are derived by first writing down the large-scale likelihood for the galaxy survey and analytically optimizing for the statistics of interest, in a manner similar to that used in early CMB and LSS analyses [e.g., [55–58]]. Schematically, the estimator for the power spectrum in some bin α (comprising a set of wave numbers and multipole) can be written:

$$\hat{p}_\alpha = \sum_\beta F^{-1}_{\alpha\beta}[\hat{q}_\beta - \bar{q}_\beta], \tag{3}$$

where $\hat{q}_\alpha$ is a quadratic piece, $\bar{q}_\alpha$ is a bias term, and $F_{\alpha\beta}$ is a Fisher matrix. These can be computed in terms of the pixelized data-vector, $\mathbf{d}$, the associated covariance matrix, $\mathsf{C} \equiv \langle \mathbf{d}\mathbf{d}^T \rangle$, and the noise covariance, N, as

$$\hat{q}_\alpha = \frac{1}{2}[\mathsf{C}^{-1}\mathbf{d}]^T \mathsf{C}_{,\alpha}[\mathsf{C}^{-1}\mathbf{d}], \qquad \bar{q}_\alpha = \frac{1}{2}\mathrm{Tr}[\mathsf{C}^{-1}\mathsf{C}_{,\alpha}\mathsf{C}^{-1}\mathsf{N}],$$
$$F_{\alpha\beta} = \frac{1}{2}\mathrm{Tr}[\mathsf{C}^{-1}\mathsf{C}_{,\alpha}\mathsf{C}^{-1}\mathsf{C}_{,\beta}], \tag{4}$$

where $\mathsf{C}_{,\alpha}$ represents the derivative of the pixel covariance with respect to the signal of interest, and we note that both C and N both depend on the survey mask. In certain limits, the first piece is proportional to the conventional FKP power spectrum, while the second removes the Poissonian noise contribution, and the third acts to deconvolve the window. A similar form can be obtained for the bispectrum components, $\{b_\alpha\}$ (where α specifies a triplet of bins):

$$\hat{b}_\alpha = \sum_\beta \mathcal{F}^{-1}_{\alpha\beta}\hat{c}_\beta, \tag{5}$$

where $\hat{c}_\alpha$ is a cubic estimator and $\mathcal{F}$ is the associated Fisher matrix (which is close to tridiagonal). These can be written in terms of the three-point expectation of the data: $\mathsf{B}^{ijk} \equiv \langle d^i d^j d^k \rangle$ (using latin indices to denote pixels and employing Einstein summation), and take the form

$$\hat{c}_\alpha = \frac{1}{6}\mathsf{B}^{ijk}_{,\alpha}[\mathsf{C}^{-1}\mathbf{d}]_i([\mathsf{C}^{-1}\mathbf{d}]_j[\mathsf{C}^{-1}\mathbf{d}]_k - 3\mathsf{C}^{-1}_{jk}),$$
$$\mathcal{F}_{\alpha\beta} = \frac{1}{6}\mathsf{B}^{ijk}_{,\alpha}\mathsf{B}^{lmn}_{,\beta}\mathsf{C}^{-1}_{il}\mathsf{C}^{-1}_{jm}\mathsf{C}^{-1}_{kn}. \tag{6}$$

Notably, $\hat{c}_\alpha$ contains a piece *linear* in the data; this is not found in conventional LSS estimators (though commonplace for the CMB [77]), and helps to reduce variance on large scales. All quantities appearing in the power spectrum and bispectrum estimators can be efficiently computed using Monte Carlo methods, and give minimum variance estimates of the spectra.

Here, we use the specific forms of the estimators suggested in [54], approximating the pixel covariance by a diagonal (FKP-like) form with $P_{\rm fkp} \approx 10^4 h^{-3}$ Mpc^3, though still fully accounting for survey geometry.[6] While this leads to a slight loss of optimality, this approximation greatly reduces computation time and does not induce bias. The estimators are implemented using a Fourier-space grid with Nyquist frequency of $k_{\rm Nyq} = 0.45h$ Mpc^{-1} ($0.3h$ Mpc^{-1}) for the power spectrum (bispectrum), measuring all modes up to $k = 0.41h$ Mpc^{-1} ($0.16h$ Mpc^{-1}) with $\Delta k = 0.005h$ Mpc^{-1}

[6]Due to a minor error in the original code, the FKP weight differs from this value at the ∼10% level; the impact of this is negligible in practice.

($0.01h$ Mpc^{-1}), and using the power spectrum monopole, quadrupole and hexadecapole. We caution that the first and last bins will be contaminated with integral-constraint and window-leakage effects respectively; these are not included in the analysis below. In total we use 100 Monte Carlo simulations to compute the Fisher matrices (which gives only a subpercent noise penalty, cf. [54]), requiring a total of ≈10000 (≈3000) CPU-hours for the power spectrum (bispectrum) of all four BOSS data chunks. Importantly, this only needs to be done once per survey geometry. The increased computation time for the power spectrum is due to both the larger number of bins (the computation time scales as $N_{\rm bins}$) and the higher-resolution grid. The data-dependent part of the power spectrum (bispectrum) estimator requires ≈15 (≈10) CPU-minutes to compute per simulation, and thus can be easily applied to all 2048 PATCHY mocks.

Using the output of the above estimators, we form the following datasets, which will be analyzed in Sec. VI (cf. Fig. 1):

(i) Redshift-space power spectrum, $P_\ell(k)$: Here, we use the power spectrum monopole, quadrupole and hexadecapole (with $\ell \in \{0,2,4\}$) with $k \in [0.01, 0.20]h$ Mpc^{-1} and $\Delta k = 0.005h$ Mpc^{-1}. Our k-space cuts are motivated by the results of [23,60]. These are corrected for the effects of survey geometry and given by the outputs of the above estimators. We use a total of 38 bins for each multipole.

(ii) Real-space power spectrum, $Q_0(k)$: Following [78] (see also the earlier works of [79,80]), we use an analog to the real-space power spectrum computed from the above redshift-space power spectrum multipoles up to $\ell = 4$, explicitly via $Q_0(k) \equiv P_0(k) - \frac{1}{2}P_2(k) + \frac{3}{8}P_4(k)$. This is included for $k \in [0.2, 0.4]h$ Mpc^{-1} (involving 40 bins) and allows cosmological information to be included without the limitations of fingers-of-God modeling.

(iii) BAO parameters, $\alpha_\parallel, \alpha_\perp$: To capture sound-horizon information present in the reconstructed power spectrum, we include the parallel and perpendicular BAO scaling parameters, as discussed in [22]. These are measured for all data chunks in the BOSS and PATCHY datasets, and correlations are included via a joint covariance matrix (see [20] for an alternative approach). We note that only 999 mocks are available for these parameters.

(iv) Bispectrum, $B_0(k_1, k_2, k_3)$: The bispectrum monopole is obtained from the above cubic estimators.[7] To avoid window leakage and poorly modelled regimes, we use only k-modes in the range $[0.01, 0.08]h$ Mpc^{-1} and $\Delta k = 0.01h$ Mpc^{-1}, whose centers satisfy the triangle condition $|k_1 - k_2| \leq k_3 \leq k_1 + k_2$ [47].[8] In total, we include 62 bispectrum bins.

Each statistic is computed for the BOSS data, the PATCHY mocks, the NSERIES mocks and the PATCHY-NSERIES mocks, and the data, estimation pipeline, and likelihoods are made publicly available online.[9] The total data-vector contains $N_{\rm bin} = 114 + 40 + 2 + 62 = 218$ elements, and is shown in Fig. 2 (cf. Sec. VI).

IV. THEORETICAL MODEL AND LIKELIHOOD

A. Theory model

To model the window-free power spectrum and bispectrum, we utilize the EFTofLSS, as implemented in the Boltzmann code CLASS-PT [81] (see also [82,83]). For consistency, the power spectrum (bispectrum) model is computed up to one-loop (tree-level) order, and both include full treatment of all necessary components, including perturbative corrections, galaxy bias, ultraviolet counterterms (to consistently account for short-scale physics), infrared resummation (to treat long-wavelength displacements) and stochasticity (including shot-noise and fingers-of-God effects). Full discussion of our models can be found in [18,60,81] for the redshift-space power spectrum, [78] for the real-space power spectrum analog, [22] for the BAO parameters, and [47] for the bispectrum.

Schematically, our model of the power spectrum multipoles takes the following form (before the effects of infrared resummation and coordinate transformations):

$$P_\ell(k) = P_\ell^{\rm tree}(k) + P_\ell^{\rm 1-loop}(k) + P_\ell^{\rm ct}(k) + P_\ell^{\rm stoch}(k), \qquad (7)$$

where the four terms are the usual linear theory Kaiser multipoles [scaling as the linear-theory power spectrum, $P_{\rm lin}(k)$], the one-loop perturbation theory corrections (scaling as $k^2 P_{\rm lin}(k)$ on large scales), the counterterms [scaling as $k^2 P_{\rm lin}(k)$], and the stochastic contributions (scaling as a constant, plus corrections), respectively. This is then resummed to correct for the action of nonperturbative long-wavelength displacements, with the effect of suppressing the wiggly part of the spectrum (see [81]). We account for the effects of an incorrect fiducial cosmology (often known, erroneously, as the Alcock-Paczynski distortion [84]) via the rescalings

[7] Strictly, the estimate of the bispectrum monopole is unbiased only if one measures all possible bispectrum multipoles, due to coupling of the redshift-space contributions with the anisotropic window function (analogous to the power spectrum case). Here, we assume this effect to be small, though its magnitude will be studied in future work.

[8] Note that triangles violating this condition must be included in the initial bispectrum estimator, to avoid bias, though they can be dropped when the statistic is analyzed.

[9] See GitHub.com/oliverphilcox/BOSS-Without-Windows and GitHub.com/oliverphilcox/full_shape_likelihoods.

$$k \to k' \equiv k\left[\left(\frac{H_{\rm true}}{H_{\rm fid}}\right)^2\mu^2 + \left(\frac{D_{A,\rm fid}}{D_{A,\rm true}}\right)^2(1-\mu^2)\right]^{1/2}$$
$$\mu \to \mu' \equiv \mu\left(\frac{H_{\rm true}}{H_{\rm fid}}\right)\left[\left(\frac{H_{\rm true}}{H_{\rm fid}}\right)^2\mu^2 + \left(\frac{D_{A,\rm fid}}{D_{A,\rm true}}\right)^2(1-\mu^2)\right]^{-1/2}, \tag{8}$$

where unprimed quantities are those measured observationally, and all quantities are evaluated at the sample redshift. The real-space power spectrum model (needed for the Q_0 statistic) is similar, but obtained by summing over the redshift-space multipoles entering (7), via $Q_0(k) = P_0(k) - \frac{1}{2}P_2(k) + \frac{3}{8}P_4(k)$.[10]

The bispectrum model can be written schematically in 3D space as

$$B(\boldsymbol{k}_1,\boldsymbol{k}_2) = B^{\rm tree}(\boldsymbol{k}_1,\boldsymbol{k}_2) + B^{\rm ct}(\boldsymbol{k}_1,\boldsymbol{k}_2) + B^{\rm stoch}(\boldsymbol{k}_1,\boldsymbol{k}_2), \tag{9}$$

corresponding to the tree-level perturbative contributions, counterterms and stochasticity respectively. While counterterms strictly appear only at one-loop, [47] found it necessary to include a $k^2\mu^2 \equiv k_\parallel^2$-like correction in the tree-level model to encapsulate fingers-of-God effects. The three terms scale as $P_{\rm lin}^2(k)$, $k_\parallel^2 P_{\rm lin}^2(k)$ and a constant plus $P_{\rm lin}(k)$. We include the effects of infrared resummation by replacing the linear matter power spectrum by its resummed version (with wiggles suppressed), and the effects of the fiducial cosmology via a redefinition of wave numbers and angles entering (9), similar to (8). The model is then integrated over external angles to obtain the bispectrum monopole, $B_0(k_1,k_2,k_3)$, which can be directly compared to data without additional window convolutions. Note that we also include a multiplicative discreteness weight, to account for the finite resolution of the Fourier-space grid [47].

B. EFTofLSS parameters

The full model for the power spectrum and bispectrum is specified by the following nuisance parameters, which appear in one or both statistics (usings the conventions described in [47]):

$$\{b_1, b_2, b_{\mathcal{G}_2}, b_{\Gamma_3}\} \times \{c_0, c_2, c_4, \tilde{c}, c_1\} \times \{P_{\rm shot}, a_0, a_2, B_{\rm shot}\} \tag{10}$$

where the first set encodes galaxy bias (from linear, quadratic, tidal, and third-order effects respectively), the second gives the counterterms for the monopole, quadrupole, and hexadecapole, fingers-of-God effect and bispectrum, while the final set accounts for the stochastic nature of the density field. Since the BOSS regions have different selection functions and calibrations, we allow the parameters to vary freely in each of the four data chunks, giving a total of 42 free parameters.

In the likelihood described below, we assume the following bias parameter priors, following [47]:

$$b_1 \in \text{flat}[0,4], \qquad b_2 \sim \mathcal{N}(0,1^2), \qquad b_{\mathcal{G}_2} \sim \mathcal{N}(0,1^2), \qquad b_{\Gamma_3} \sim \mathcal{N}\left(\frac{23}{42}(b_1-1), 1^2\right), \tag{11}$$

where $\mathcal{N}(\mu,\sigma^2)$ indicates a Gaussian distribution with mean μ and variance σ^2. Similarly, we use Gaussian priors for the counterterms and stochasticity parameters:

$$\frac{c_0}{[\text{Mpc}/h]^2} \sim \mathcal{N}(0,30^2), \qquad \frac{c_2}{[\text{Mpc}/h]^2} \sim \mathcal{N}(30,30^2), \qquad \frac{c_4}{[\text{Mpc}/h]^2} \sim \mathcal{N}(0,30^2), \qquad \frac{\tilde{c}}{[\text{Mpc}/h]^4} \sim \mathcal{N}(500,500^2),$$
$$\frac{c_1}{[\text{Mpc}/h]^2} \sim \mathcal{N}(0,50^2), \qquad P_{\rm shot} \sim \mathcal{N}(0,2^2), \qquad a_0 \sim \mathcal{N}(0,2^2), \qquad a_2 \sim \mathcal{N}(0,2^2), \qquad B_{\rm shot} \sim \mathcal{N}(1,2^2). \tag{12}$$

In our conventions, the stochastic contributions are specified by the scale-dependent spectra, $P_{\rm stoch}$ and $B_{\rm stoch}$, with

$$P_{\rm stoch}(k) = \frac{1}{\bar{n}}\left[1 + P_{\rm shot} + a_0\left(\frac{k}{k_{\rm NL}}\right)^2 + a_2\mu^2\left(\frac{k}{k_{\rm NL}}\right)^2\right],$$
$$B_{\rm stoch}(k_1,k_2,k_3) = \frac{B_{\rm shot}}{\bar{n}}\left[Z_1(\mathbf{k}_1)(b_1 + b_\eta f\mu_1^2)P^{\rm tree}(k_1) + \text{cycl.}\right] + \frac{1}{\bar{n}^2}(1+P_{\rm shot})^2, \tag{13}$$

for nonlinear scale $k_{\rm NL} = 0.45h$ Mpc^{-1}, redshift-space kernel $Z_1(\boldsymbol{k})$, number density $\bar{n} \approx 3\times 10^{-4}h^3$ Mpc^{-3}, and $b_\eta = (1+P_{\rm shot})/(B_{\rm shot})$.

[10]Note that this is not quite equal to the real-space power spectrum (i.e., that with $f = 0$) due to infrared resummation effects.

C. Likelihood

Given that our analysis primarily concerns large-scale density modes, we will assume a Gaussian likelihood for the data-vector $\mathbf{d}$ (comprising the power spectrum multipoles, the real-space power spectrum Q_0, the BAO parameters, and the bispectrum), given some set of parameters $\mathbf{p}$:

$$-2\log\mathcal{L}(\mathbf{d}|\mathbf{p}) = (\mathbf{m}(\mathbf{p})-\mathbf{d})^T\mathsf{C}^{-1}(\mathbf{m}(\mathbf{p})-\mathbf{d}) + \log|2\pi\mathsf{C}|, \tag{14}$$

where $\mathbf{m}(\mathbf{p})$ is the model prediction. The covariance matrix C (including all cross-correlations) is computed using a set of $N_{\rm mocks} = 2048$ PATCHY simulations:

$$\mathsf{C} = \frac{1}{N_{\rm mocks}-1}\sum_{k=1}^{N_{\rm mocks}}(\mathbf{d}^k-\bar{\mathbf{d}})(\mathbf{d}^k-\bar{\mathbf{d}})^T, \tag{15}$$

where $\mathbf{d}^k$ is the (stacked) data-vector from the kth mock, and $\bar{\mathbf{d}}$ the average over mocks. We include also a Hartlap correction factor to debias the estimate of the inverse covariance [85], setting $\mathsf{C}^{-1} \to (N_{\rm mocks}-N_{\rm bins}-2)/(N_{\rm mocks}-1)\times\mathsf{C}^{-1}$.[11] When the BAO parameters are included in the analysis (obtained from reconstructed power spectrum data), $N_{\rm mocks}$ is reduced to 999, slightly increasing the Hartlap factor. An alternative approach would be to compute the covariance matrix analytically [52,87]; this naturally avoids sampling noise.

In the analyses below, we vary the following cosmological parameters[12]:

$$\{h, \ln(10^{10}A_s), \omega_{\rm cdm}, \omega_b, n_s\}, \tag{16}$$

from which we can obtain the derived parameters H_0, Ω_m and σ_8. Following *Planck*, we fix the neutrino mass to $\sum m_\nu = 0.06$ eV when analyzing BOSS data (or zero for PATCHY simulations, matching the true value); this is done only for simplicity, and a full discussion of the impact of the bispectrum on neutrino mass measurement will be presented in future work. To convert the likelihood of (14) to a posterior, we require priors for all parameters: here we adopt flat priors on the cosmological parameters with infinite support, and use the priors given in Sec. IV B for the bias, counterterm and stochasticity parameters. Parameters that enter the theoretical model linearly, such as $P_{\rm shot}$, are marginalized over analytically, as in [89]; this reduces the dimensionality and allows for faster sampling. To compute the parameter posteriors, we employ a Markov Chain Monte Carlo (MCMC) analysis, implemented within the MONTEPYTHON code [90]. Sampling is performed across a number of parallel chains and assumed to converge when the Gelman-Rubin diagnostic satisfies $R < 0.03$ for all parameters. Typically, this requires ≈500 CPU-hours.

[11]This correction is strictly an approximation; properly one should account for noise in the covariance matrix by replacing the likelihood of (14) with the modified t-distribution of [86]. Here, we are in the limit of $N_{\rm mocks} \gg N_{\rm bins}$, thus this has little effect, and we do not include it since it complicates the analytic marginalization over nuisance parameters.

[12]Strictly speaking, we also fix the CMB temperature monopole T_0 to the FIRAS best-fit value. The effect of T_0 on cosmological observables has been studied in [88].

V. CONSISTENCY TESTS

Before presenting the main results of this work, we first test our pipeline by applying the estimators of Sec. III to the NSERIES simulations discussed in Sec. II. In particular, we perform a full parameter inference study using likelihood described in Sec. IV, with the data-vector given by the mean of 84 pseudoindependent NSERIES mocks, including the power spectrum multipoles, the real-space power spectrum proxy, and the bispectrum monopole. As in Sec. II, we use a covariance matrix formed from 2048 PATCHY-NSERIES mocks, whose window function matches that of the CMASS NGC region.

Two analyses are performed: (1), with the covariance rescaled by a factor of 84 to give an effective volume equivalent to that of the total NSERIES suite ($V_{\rm eff} = 235h^{-3}$ Gpc^3), and (2), with the covariance rescaled by a factor of 2.4, matching the total effective volume of BOSS DR12 ($V_{\rm eff} = 6h^{-3}$ Gpc^3). The first allows us to quantify the systematic errors given our choice of scale-cuts, while the second helps to assess the prior volume shifts arising from nuisance parameter marginalizations. We caution that the two sources of bias are very different in nature: the theoretical systematics are generated by truncating the perturbative expansion at a given order, while the prior volume effect appears due to the need to marginalize nuisance parameters over poorly known priors. In the limit of infinite data, i.e., when nuisance parameters are determined by the data itself and not by the priors, the best-fit cosmological parameters will equal their true values if systematic effects can be ignored. We caution also that non-Gaussianity of the posterior can lead to mean values shifted with respect to the best-fits, even in the absence of priors and systematic errors.

A corner plot of the resulting parameter constraints is shown in Fig. 3, with one-dimensional marginalized limits given in Table II. When considering the BOSS-scaled covarinace, we find that all cosmological parameters are correctly recovered within 68% confidence level (CL); indeed, the parameter shifts are much smaller than 1σ in most cases, indicating that our joint power spectrum and bispectrum analysis is producing accurate parameter estimates. Considering the full simulation volume, we find that all parameters are recovered within the 95% CL, with largest discrepancies found for n_s and σ_8. The residual shifts can be conservatively attributed to systematic limitations of our theoretical model, arising from

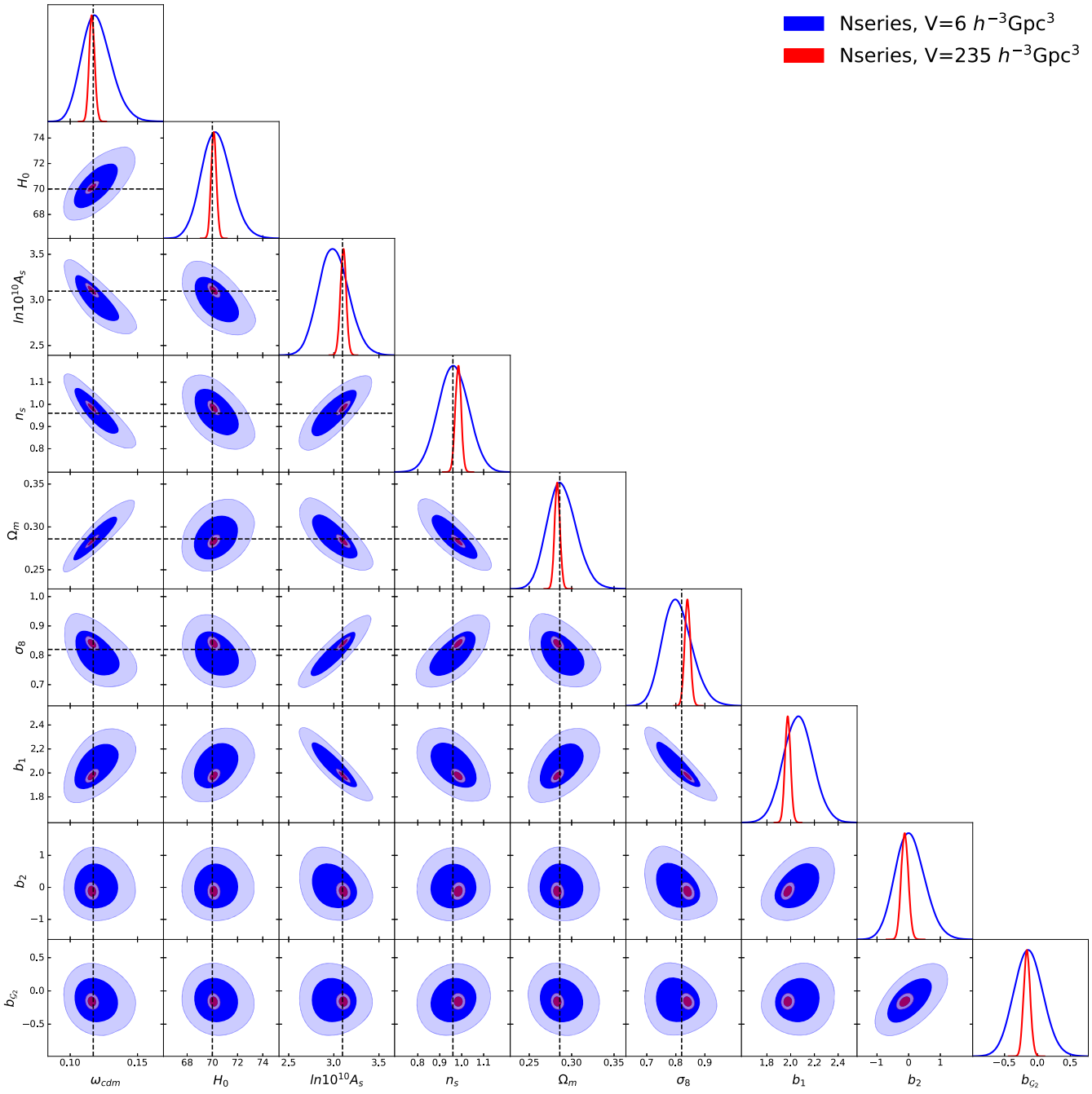

FIG. 3. Constraints on cosmological and bias parameters extracted from the power spectrum and bispectrum of 84 NSERIES simulations, with a covariance matrix rescaled to match the total volume of BOSS (blue), and that of the NSERIES suite (red). Dashed lines mark fiducial values of cosmological parameters, and we give the marginalized limits in Table II. Notably, any systematic effects are strongly subdominant for the BOSS-scaled posteriors, though there are slight shifts for the full NSERIES volume (which is somewhat larger than the full DESI dataset).

higher-order perturbative terms, or small inaccuracies in our window function treatment. We caution that the NSERIES volume is larger even than the full DESI sample, and further, that the 84 NSERIES mocks are not fully independent (since they are generated from the same N-body simulations), thus the above shifts are necessarily an overestimate.

The largest systematic shift is observed for σ_8, which, if one rescales the full NSERIES-volume constraint to the BOSS volume, reaches the level of 0.4σ. While not insignificant, this is likely inflated by (a) the nonindependence of the NSERIES mocks, and (b), the non-Gaussianity of the posterior surface, which will drive the mean away from the best-fit value. We may also consider the marginalization

TABLE II. Marginalized constraints on key cosmological and bias parameters extracted from the mean of 84 NSERIES simulations, analyzed covariances corresponding to the BOSS volume (top) and the total NSERIES volume (bottom). In all cases, the analysis uses the power spectrum multipoles up to $k_{\rm max} = 0.2h$ Mpc^{-1}, the real-space power spectrum up to $k_{\rm max} = 0.4h$ Mpc^{-1}, and the bispectrum up to $k_{\rm max} = 0.08h$ Mpc^{-1}. The fiducial cosmology is given by $\omega_{\rm cdm} = 0.1171$, $H_0 = 70$ km s^{-1} Mpc^{-1}, $n_s = 0.96$, $\ln(10^{10}A_s) = 3.091$, $\Omega_m = 0.286$, and $\sigma_8 = 0.82$. The two-dimensional posterior is shown in Fig. 3.

Volume	$\omega_{\rm cdm}$	H_0	n_s	$\ln(10^{10}A_s)$	Ω_m	σ_8	b_1	b_2	$b_{\mathcal{G}_2}$
$6h^{-3}$ Gpc^3	$0.119^{+0.010}_{-0.012}$	$70.3^{+1.1}_{-1.3}$	$0.965^{+0.068}_{-0.071}$	$3.01^{+0.16}_{-0.17}$	$0.288^{+0.016}_{-0.018}$	$0.808^{+0.047}_{-0.054}$	$2.06^{+0.12}_{-0.13}$	$0.04^{+0.43}_{-0.52}$	$-0.14^{+0.22}_{-0.23}$
$235h^{-3}$ Gpc^3	$0.1161^{+0.0020}_{-0.0022}$	$70.11^{+0.20}_{-0.22}$	$0.984^{+0.014}_{-0.013}$	$3.105^{+0.033}_{-0.032}$	$0.2831^{+0.0032}_{-0.0033}$	$0.84^{+0.01}_{-0.01}$	$1.98^{+0.023}_{-0.024}$	$-0.12^{+0.11}_{-0.12}$	$-0.16^{+0.050}_{-0.052}$

bias, i.e., the difference between the means in the two analyses; this is equal to 0.6σ for σ_8 (using BOSS error bars) and less than 0.3σ for other parameters. These two biases cancel each other for σ_8, such that the resulting shift is only 0.2σ. These results agree with previous studies [23,47], and allow us to conclude that our analysis pipeline, with the chosen k-space cuts, is robust and may be applied to BOSS data to yield accurate parameter constraints. Given that the NSERIES volume is several times larger than that of DESI, and the combined covariance is an underestimate (due to the independence considerations), we expect that the current analysis could be similarly applied to future surveys.

VI. PARAMETER CONSTRAINTS FROM BOSS

Below, we present the key results of this work: parameter constraints from the full BOSS DR12 dataset, including the power spectrum (both pre- and post-reconstruction), and the bispectrum. The observational data used in this work is shown in Fig. 2 for the two redshift-slices for both BOSS and PATCHY; while the large-scale power spectrum and bispectrum are generally in agreement, we note differences between the mocks and data at larger-k, particularly for the z3 power spectrum. This matches that found in previous works [7,18], and is a consequence of the lack of small-scale matching, and simplified halo physics treatments in the PATCHY mocks.

Figure 4 shows the corresponding correlation matrices, including all datasets considered in this work. Notably, we do not find strong correlations between the various statistics, aside from those in $P_\ell(k)$ and $P_{\ell'}(k)$, which are expected from linear theory. That the correlations are weaker than those found previously [7,7,22] is also of no surprise: much of the large-scale correlations is imprinted by the window function, and will be

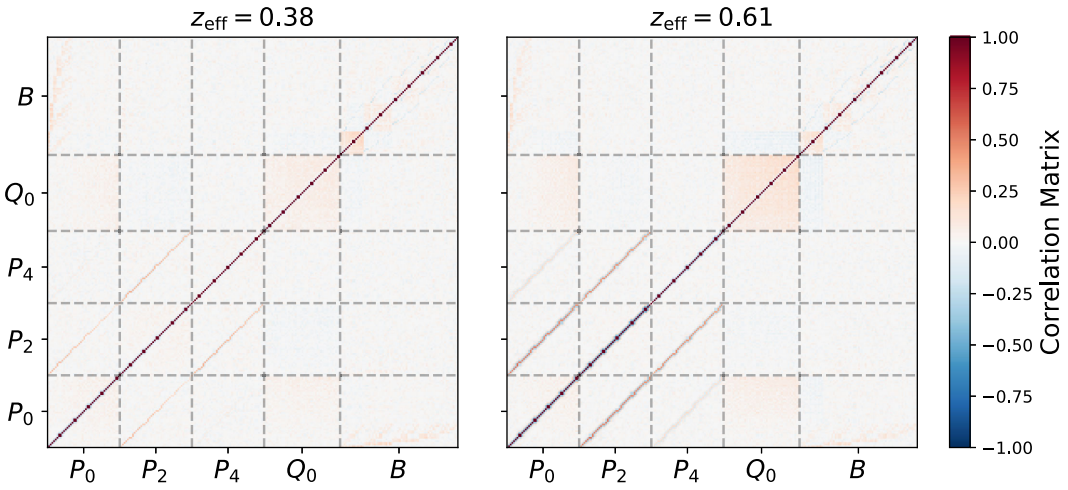

FIG. 4. Correlation matrices for the power spectrum and bispectrum measurements used in this work, computed using 2048 PATCHY simulations. The left (right) plot gives the result for the z1 (z3) redshift slice, averaging together NGC and SGC measurements for visibility, as in Fig. 2. The correlation matrix is defined $R_{ij} \equiv C_{ij}/\sqrt{C_{ii}C_{jj}}$ for covariance C_{ij}. Here the first through third submatrices show the results from the power spectrum monopole, quadrupole and hexadecapole respectively, the fourth gives the result from the real-space power spectrum, Q_0, while the fifth gives that from the bispectrum. For clarity, we omit the BAO parameters, whose covariance with the windowed spectra can be found in [22]. In each case, we include only k-modes used in the analysis below; i.e., we use $0.01 \le k \le 0.20$ for P_ℓ, $0.20 \le k \le 0.4$ for Q_0 and $0.01 \le k \le 0.08$ for B_0 (in hMpc^{-1} units). In general, there is little off-diagonal correlation, except for the Q_0 statistic which involves smaller scale information. Note that the correlation is less than conventionally found, since our measurements are not window convolved; however, the z1 and z3 covariances appear somewhat different, due to both the different redshift, and selection functions of the two.

substantially reduced by the window-free estimators of Sec. III [53,54]. We do however observe stronger correlations between bins in the real-space power spectrum Q_0: this occurs since this statistic includes smaller scales, whence the off-diagonal trispectrum covariance becomes important. Since we use only mock-based covariances, such higher-order couplings are naturally included in the analysis.

A. Baseline analysis

1. Results

We begin by analyzing the power spectrum, BAO parameters, and bispectrum in the manner described above, with all cosmological parameters (except the neutrino mass) free. The main results of this are displayed in Fig. 5 (and summarized in Fig. 1), with the associated

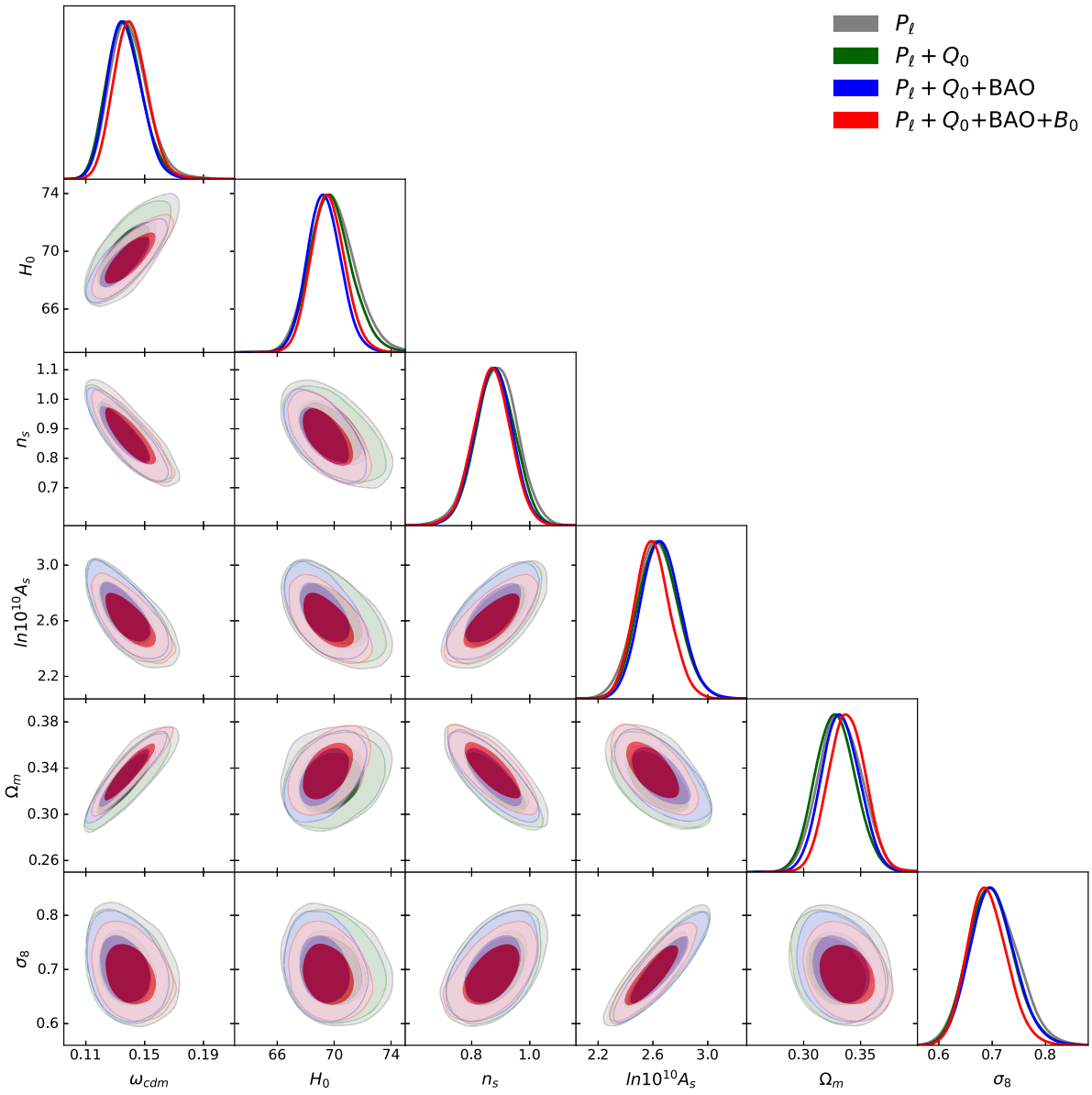

FIG. 5. Cosmological parameter constraints from the ΛCDM analysis of BOSS data, including the power spectrum (P_ℓ), real-space power spectrum analog (Q_0), BAO parameters from reconstructed spectra (BAO), and the bispectrum monopole (B_0). The marginalized constraints are given in Table III. As found previously, the addition of Q_0 gives a slight decrease in the posterior volume (limited mostly by shot-noise), while BAO parameters help to reduce the H_0 contour, and the bispectrum gives a 13% reduction in the σ_8 error bar. Notably, the spectral slope is poorly constrained and degenerate with other parameters; results with a *Planck* prior on n_s are shown in Fig. 6.

TABLE III. Cosmological parameter constraints from the ΛCDM analysis of BOSS using the power spectrum multipoles, real-space power spectrum, BAO parameters, and bispectrum. For each analysis, we display mean values and 68% confidence intervals. A BBN prior on the physical baryon density ω_b is assumed in all cases, and the corresponding posterior is not displayed. The left group of parameters are those directly sampled in the MCMC chains, while those on the right are derived parameters. A corner plot of these results is given in Fig. 5, and bias parameter constraints from the final two datasets are shown in Appendix.

Dataset	$\omega_{\rm cdm}$	h	$\ln(10^{10}A_s)$	n_s	Ω_m	σ_8
$P_\ell(k)$	$0.139^{+0.011}_{-0.015}$	$0.699^{+0.015}_{-0.017}$	$2.63^{+0.15}_{-0.16}$	$0.883^{+0.076}_{-0.072}$	$0.333^{+0.019}_{-0.020}$	$0.704^{+0.044}_{-0.049}$
$P_\ell(k)+Q_0(k)$	$0.137^{+0.011}_{-0.014}$	$0.698^{+0.013}_{-0.016}$	$2.64^{+0.14}_{-0.16}$	$0.880^{+0.068}_{-0.068}$	$0.328^{+0.017}_{-0.019}$	$0.699^{+0.040}_{-0.046}$
$P_\ell(k)+Q_0(k)+\mathrm{BAO}$	$0.137^{+0.011}_{-0.013}$	$0.693^{+0.011}_{-0.013}$	$2.66^{+0.14}_{-0.15}$	$0.874^{+0.067}_{-0.064}$	$0.333^{+0.016}_{-0.018}$	$0.701^{+0.040}_{-0.045}$
$P_\ell(k)+Q_0(k)+\mathrm{BAO}+B_0$	$0.141^{+0.011}_{-0.013}$	$0.696^{+0.011}_{-0.013}$	$2.60^{+0.13}_{-0.14}$	$0.870^{+0.067}_{-0.064}$	$0.338^{+0.016}_{-0.017}$	$0.692^{+0.035}_{-0.041}$

parameter confidence intervals given in Table III, with additional results (including best-fits, 95% confidence levels, and full corner plots including bias parameters) given in Appendix. As more datasets are included in the analysis, we find that the mean parameter values are generally consistent, but the error bars reduce.

The addition of Q_0 gives a slight improvement in the precision with which a variety of parameters can be measured; this arises due to the inclusion of smaller-scale power spectrum information, the importance of which is limited by the high BOSS shot-noise [78]. When BAO parameters are included, the H_0 contour shrinks by approximately 20%, matching the conclusion of [22]. Here, the extra constraining power is sourced by higher-order statistics, whose sound-horizon information is transferred to the power spectrum, following BAO reconstruction [16]. Finally, when we add the bispectrum monopole, the σ_8 posterior shrinks by 13% (in accordance with the N-body results of [47]), though other projections remain consistent. In this case, information arises from broadband features in the bispectrum, and allows for degeneracy breaking, which acts to tight the constraint on the fluctuation amplitude. Notably, the H_0 posterior is not tightened—this occurs since the large-scale bispectrum does not include BAO signatures (since we truncate at $k = 0.08h$ Mpc^{-1}). Information present on smaller scales is already included via the BAO parameters (see [17] for a detection of this from the three-point function alone). Although the bispectrum is not found to give particularly large improvements in the error bars of cosmological parameters, this is primarily due to our conservative choices of $k_{\rm max}$ and bias parameter priors, and would change if one accepted a larger systematic error budget or developed the theoretical modeling further [47]. If one is instead interested in galaxy formation physics, the bispectrum's addition improves constraints significantly; this is discussed in Sec. VI D.

2. Cosmological interpretation

The parameter contours found above can be straightforwardly compared to those of other analyses, both making use of LSS data, and other sources. For the Hubble constant, we find a marginalized constraint of $H_0 = 69.6^{+1.1}_{-1.3}$ km s^{-1} Mpc^{-1} when all datasets are combined. This is consistent with that reported in [47] (using P_ℓ and Q_0 information), but somewhat higher than the results of [18,22]. The difference is thought to arise from the power spectrum measurements themselves: in this work, and [47], we do not use public data products, but instead remeasure the spectra from scratch (cf. Sec. VI B 2). Here, this is achieved via window-free estimators, which Sec. V show to give robust parameter constraints. Our H_0 posterior is somewhat lower than those obtained from the Cepheid-calibrated distance ladder [91]: $H_0^{\rm SH0ES} = 73.2 \pm 1.3$ km s^{-1} Mpc^{-1}, though, given the large error bars, it is difficult to draw any firm conclusions. The Ω_m posterior is consistent with that of the Pantheon sample: $\Omega_m^{\rm Pantheon} = 0.298 \pm 0.022$ [92], and the n_s posterior is broad, but in agreement with that from *Planck*: $n_s^{\rm Planck} = 0.9649 \pm 0.0042$.

The σ_8 results are of particular interest. Our full analysis finds $\sigma_8 = 0.69 \pm 0.04$ (or $\sigma_8 = 0.70 \pm 0.05$, using the power spectrum multipoles alone), which is somewhat different from that of previous full-shape power spectrum analyses [18,19,21,28]. Comparison with the old analyses in not straightforward, since they differ in many aspects, such as the inclusion of the hexadecapole moment in the data and window function model, the choice of sampling parameters, e.g., whether to use $A_s/A_{s,\rm Planck}$ or $\ln(10^{10}A_s)$, and finally, the priors on nuisance parameters. If we analyze the power spectrum data used by the former works with the same theory model and data cuts as our baseline analysis (see Sec. VI B 2), and consistently treat the window function, we find $\sigma_8 = 0.66 \pm 0.05$, which is significantly lower than the *Planck* value, and 1σ below our current bound.

This difference is entirely caused by an error in the public BOSS power spectra.[13] whereupon the spectra were incorrectly suppressed by a constant factor ≈10%. This occurred due to an invalid approximation in the power spectrum normalization: the geometric factor $A \equiv \int d\boldsymbol{r}\bar{n}^2(\boldsymbol{r})w_{\rm fkp}^2(\boldsymbol{r})$

[13]Available at fbeutler.GitHub.io/hub/boss_papers.html.

appearing in the standard FKP power spectrum estimator was replaced by a sum over random particles:

$$A_{\rm approx} = \frac{N_{\rm g}}{N_{\rm r}} \sum_{i \in {\rm randoms}} \bar{n}_g(z_i) w_{{\rm fkp},i}^2, \tag{17}$$

for approximate redshift dependence $\bar{n}_g(z_i)$, using a (weighted) total of $N_{\rm gal}$ galaxies and $N_{\rm rand}$ randoms [7,11,12,21]. This approximation is valid only at the ≈10% level for the BOSS sample, and the power spectra should strictly be normalized by the $r \to 0$ limit of the window function $W(r)$ (which is equal to the two-point correlation function of the random particles) [8,93].[14] At linear order, $P(k,\mu) \propto [b + f\mu^2]^2\sigma_8^2$, thus this has the effect of reducing the value of σ_8 by ∼5% relative to its true value. This resulted in a a series of works that found σ_8 to be in (erroneous) mild tension with *Planck*. In our approach, we do not require the 2PCF of the mask to be computed explicitly, thus are not affected by such problems. Our results for σ_8 are consistent with those found in [20], which uses the correctly normalized spectra.

Recent works have found a growing tendency for weak-lensing analyses to predict lower clustering amplitudes than that of *Planck*; an anomaly that shows greater consistency between observables than the much-ballyhooed 'H_0 tension'. In terms of the $S_8 \equiv \sigma_8(\Omega_m/0.3)^{0.5}$ parameter, *Planck* finds $S_8^{\rm Planck} = 0.832 \pm 0.012$ [73], while the latest weak lensing results from the latest Dark Energy Survey 3×2 analysis finds $S_8^{\rm DES} = 0.776 \pm 0.017$ [95]. An additional constraint is obtained from cross-correlating galaxy surveys with the CMB: this obtained $S_8 = 0.776 \pm 0.017$ for the unWISE sample [96], and $S_8 = 0.73 \pm 0.03$ when using the DESI imaging survey [97]. Here, we find $S_8 = 0.734^{+0.035}_{-0.041}$; this is consistent with the other low-redshift observations, but differs from *Planck* at the 2.5σ level. The upcoming tranche of spectroscopic and photometric survey data will be able to shed light on whether this is indeed a *bona fide* discrepancy (the prospect of which is discussed in Sec. VI C), or simply a statistical fluctuation.

B. Analysis with fixed n_s

1. Results

Spectroscopic surveys generally lead to poor constraints on the primordial slope, n_s, due to the limited survey size, and thus the resolution of large-scale modes. For this reason, many analyses have opted to fix n_s by imposing a tight Gaussian prior on n_s, with width given by the *Planck* constraints [73]. To allow straightforward comparison with previous works, we additionally perform the analysis described above using the n_s-prior, the results of which are shown in Fig. 6 and Table IV, with additional constraints displayed in Appendix.

Our conclusions in this case are similar to before: the inclusion of Q_0 leads to a slight reduction in parameter variances, BAO tightens the H_0 posterior by ≈20%, and B_0 sharpens the σ_8 constraint by 13%. Including a highly restrictive prior on n_s reduces a number of parameter degeneracies, improving the precision with which Ω_m can be measured by almost 40%. For H_0, we find a posterior of $68.3^{+0.8}_{-0.9}$ km s^{-1} Mpc^{-1} when all datasets are included, which is closer to the *Planck* result, and further from that of Cepheid-calibrated supernovae. For σ_8, the marginalized constraint becomes $0.72^{+0.03}_{-0.04}$, now with an error below <5%, while S_8 is given by 0.751 ± 0.039, now within 2σ of *Planck*. We caution that these shifts are a natural phenomenon of non-Gaussian posteriors, and are not an indication of some failure of the cosmological model. Indeed, from Fig. 5 it is evident that the value of n_s preferred by *Planck* is higher than that directly inferred from the BOSS data. As such, imposing the *Planck* n_s prior pulls σ_8 to larger values due to the variables' positive correlation. This explains the small upward shift in σ_8 and S_8, which reduces the tension with *Planck*.

2. Comparison to other power spectrum analyses

As an additional test of our pipeline, we compare our results to those obtained using the publicly available BOSS DR12 power spectrum measurements (corrected for the normalization issue discussed in Sec. VI A 2). For this purpose, we reanalyze the public data using the same theory model and data-cuts described above, but restricting to the power spectrum multipoles, and including the window function in the theory model (as in [18]). This ensures that the analyses differ only due to the underlying power spectra and covariance matrix.

As shown in Table IV and Fig. 7, we find a close-to-perfect agreement between the two analyses, with the only noticeable difference being a $\lesssim 0.5\sigma$ downward shift of $\omega_{\rm cdm}$, which, in turn, pulls A_s upwards due to an anti-correlation.[15] The shift is insignificant at the level of the current data, and could be caused either by a inaccuracy in the window function modeling in the public data, or a residual measurement systematic in the new approach (though the latter was found to produce highly accurate $\omega_{\rm cdm}$ estimates in Sec. V). This shift is also similar to the 0.5σ bias on $\omega_{\rm cdm}$ found to arise from noise in the sample covariance matrix in [89,98]. In this regard, it is important to note that the public covariance matrices use k-bins of width $\Delta k = 0.01h$ Mpc^{-1}, which is twice as large as our

[14] We caution that this normalization is still used in the NBODYKIT code [94], and was also present in the reanalysis of [78]. To correct for it, one must similarly normalize the window function by $A_{\rm approx}$, instead of the usual approach, which sets $\lim_{r\to 0} W(r) = 1$.

[15] Note that $\omega_{\rm cdm}$ is measured directly from the broadband shape of the monopole, while A_s is primarily derived from $f\sigma_8$, rather than being measured directly from the full-shape data [18].

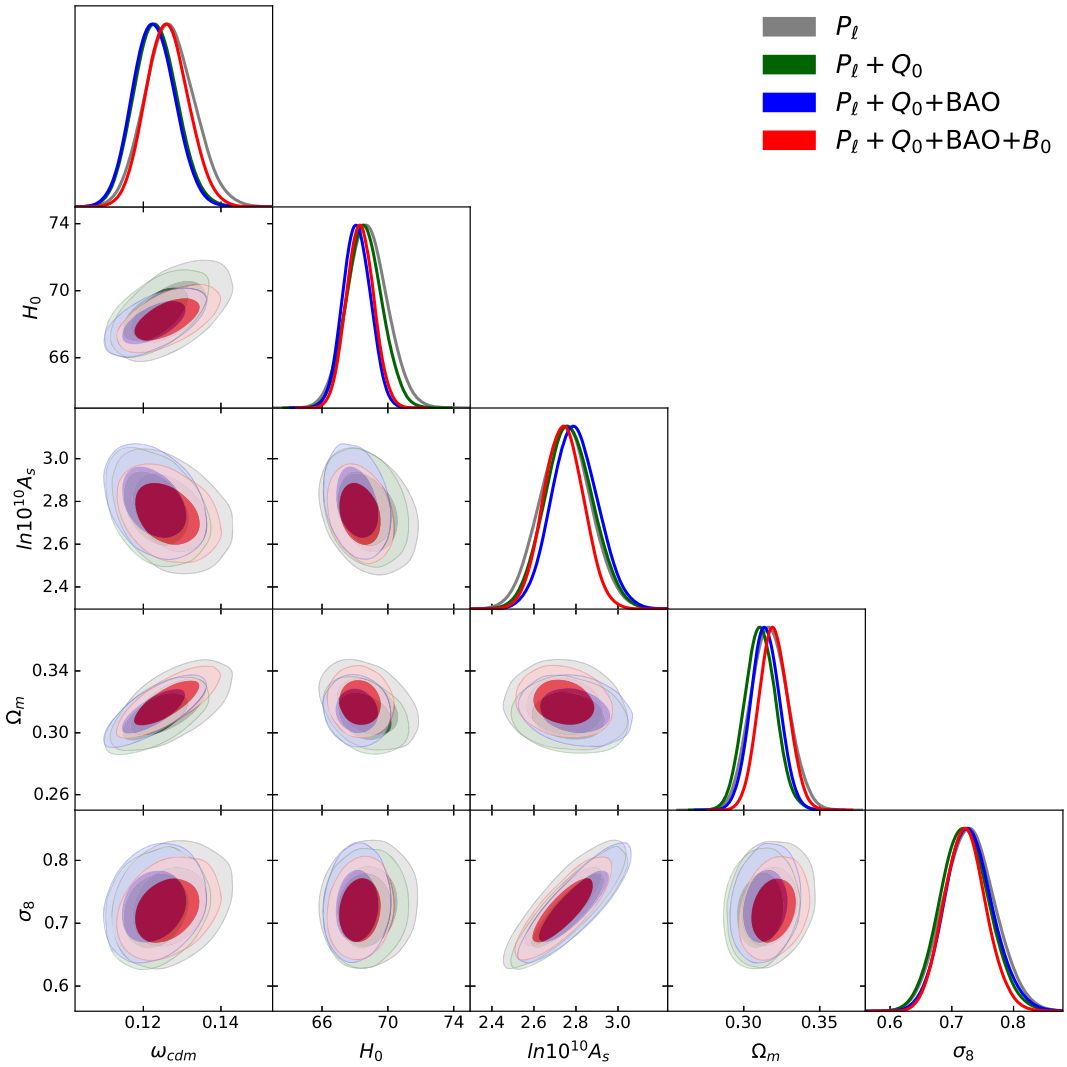

FIG. 6. As Fig. 5, but with a *Planck* prior on the spectra slope n_s. Our conclusions are broadly consistent with that of the free-n_s analysis, but feature somewhat tighter parameter constraints. The corresponding marginalized posteriors are shown in Table IV.

choice. Although we do not expect the binning to affect the power spectrum model, it will modify the noise properties of the covariance, since it changes the number of data points for a given number of mocks. A thorough investigation of this issue goes beyond the scope of this paper.

We may also compare the results of this section with other recent full-shape analyses that include the *Planck* prior on the spectral tilt. In particular, our results are in good agreement with [20], which analyzed the (corrected) public BOSS DR12 power spectra using a similar

TABLE IV. As Table III, but including a *Planck* prior on n_s. The corresponding corner plot is given in Fig. 6. We additionally include the results of a windowed analysis of the public BOSS power spectrum (top line); this is described in Sec. VI B 2 and provides a useful test of our analysis pipeline.

Dataset	$\omega_{\rm cdm}$	h	$\ln(10^{10}A_s)$	Ω_m	σ_8
$P_\ell(k)$, public	$0.1233^{+0.0058}_{-0.0065}$	$0.685^{+0.011}_{-0.013}$	$2.81^{+0.12}_{-0.12}$	$0.312^{+0.011}_{-0.012}$	$0.737^{+0.040}_{-0.044}$
$P_\ell(k)$	$0.1268^{+0.0062}_{-0.0068}$	$0.688^{+0.012}_{-0.013}$	$2.75^{+0.12}_{-0.13}$	$0.317^{+0.012}_{-0.013}$	$0.729^{+0.040}_{-0.045}$
$P_\ell(k) + Q_0(k)$	$0.1232^{+0.0054}_{-0.0058}$	$0.686^{+0.011}_{-0.011}$	$2.77^{+0.11}_{-0.12}$	$0.311^{+0.010}_{-0.010}$	$0.722^{+0.037}_{-0.042}$
$P_\ell(k) + Q_0(k) + \text{BAO}$	$0.1227^{+0.0053}_{-0.0059}$	$0.6811^{+0.0083}_{-0.0089}$	$2.80^{+0.11}_{-0.12}$	$0.314^{+0.010}_{-0.010}$	$0.729^{+0.036}_{-0.042}$
$P_\ell(k) + Q_0(k) + \text{BAO} + B_0$	$0.1262^{+0.0053}_{-0.0059}$	$0.6831^{+0.0083}_{-0.0086}$	$2.741^{+0.096}_{-0.098}$	$0.320^{+0.010}_{-0.010}$	$0.722^{+0.032}_{-0.036}$

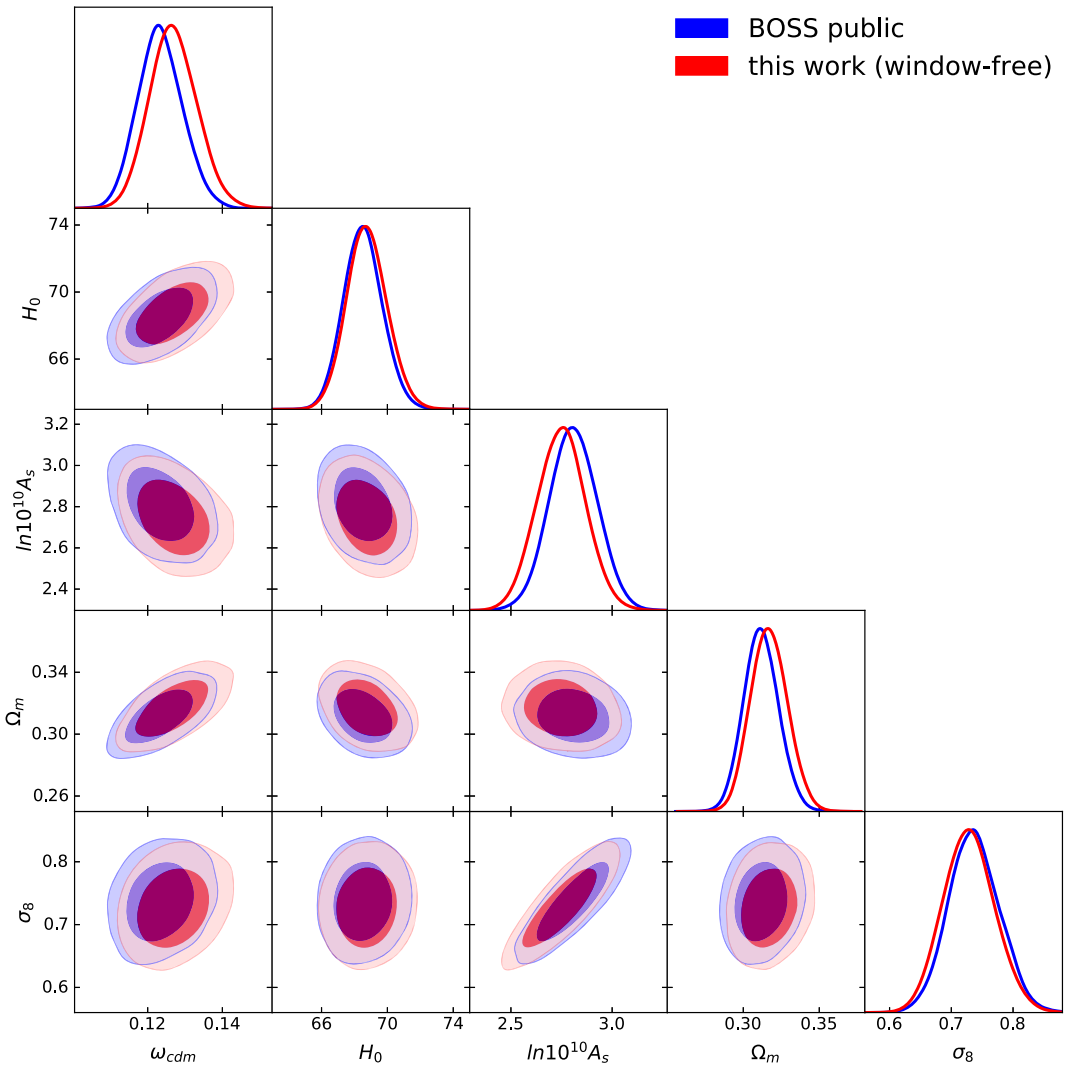

FIG. 7. Comparison of cosmological posteriors obtained from an analysis of the BOSS power spectrum using the window-free estimators of this work to that using public (windowed) BOSS data. We adopt the same theory model and scale-cuts in each case, such that differences can arise only due to the underlying data and associated covariance matrices. Our results are generally in good agreement, though our analyses find a slightly increased $\omega_{\rm cdm}$ (and thus a reduced and A_s, due to a strong anticorrelation). This is likely caused by the different window function treatments and k-space binning.

perturbation theory model and data cuts. In particular, the former work found $\sigma_8 = 0.733 \pm 0.047$, in close agreement with Table VII. Given that the two methods use different window function treatments and distinct flavors of perturbation theory, this is a useful validation of our power spectrum analysis.

An additional comparison is between our work and that of [21], which used an emulator-based approach to analyze the public BOSS data. Although the underlying model is very different to our approach, the posterior means and variances agree quite well except for σ_8, for which [21] finds a somewhat larger value, inconsistent with [20] and that of this work. As pointed out by [20] (and Sec. VI C), the σ_8 posterior is determined by large scales, $k \lesssim 0.1h$ Mpc^{-1}, thus the difference between our results is unlikely to be due to the treatment of nonlinear corrections. Given the significant difference between our methodologies, a thorough investigation of this discrepancy requires significant work. We hope to address these shifts further in the future.

C. On the plausibility of new physics

To shed light on possible tensions between our results and those of *Planck*, it is instructive to consider how our best-fit model depends on σ_8. This is shown in Fig. 8: in the left panel we plot the power spectrum monopole and quadrupole for two values of σ_8, chosen such that the resulting model has a $\Delta\chi^2$ of unity with respect to the best-fit. Notably, we observe significant changes only in the large-scale quadrupole ($k \lesssim 0.1h$ Mpc^{-1}), implying that it

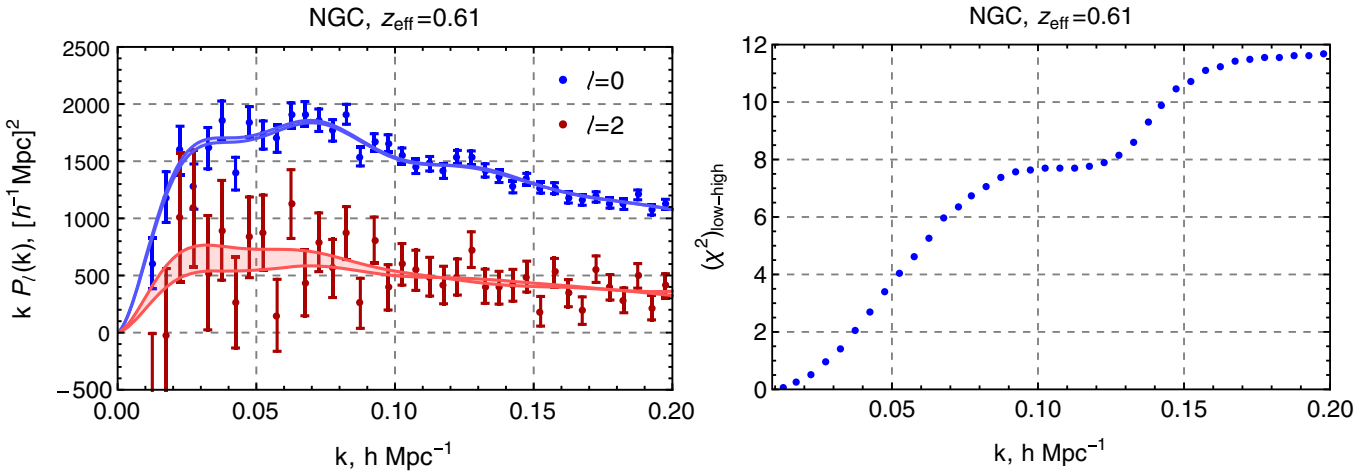

FIG. 8. Left panel: variations in the power spectrum multipoles induced by changing σ_8 to values with $\Delta\chi^2 = 1$ compared to the best-fit model, corresponding to $\sigma_8 = 0.57$ (bottom) and $\sigma_8 = 0.83$ (top), keeping other parameters fixed. For clarity, we plot only the power spectrum monopole (blue) and quadrupole (red) from the NGC 'z3' region, with error bars obtained from the PATCHY mocks. Note that there are nontrivial correlations between data-points. Right panel: cumulative χ^2 difference between the theory models with high and low σ_8 as a function of scale, *i.e.*, $[P_{\sigma_8=0.57}(k_i) - P_{\sigma_8=0.83}(k_i)]{\sf C}^{-1}_{ij}[P_{\sigma_8=0.57}(k_j) - P_{\sigma_8=0.83}(k_j)]$. Notably, this is dominated by scales with $k \lesssim 0.1h$ Mpc^{-1}.

is this region that drives our σ_8 constraints. In the right panel of Fig. 8 we show the cumulative χ^2 between the models with $\sigma_8 = 0.57$ and $\sigma_8 = 0.83$ as a function of $k_{\rm max}$. This metric is equivalent to the signal-to-noise ratio corresponding to a detection of the difference between the two models. The total χ^2 deviation between the two models is $\approx$12, the majority of which is accumulated from $k < 0.1h$ Mpc^{-1}: the χ^2 difference grows monotonically in this range, reaffirming our notion that these scales are most important for distinguishing between models with different clustering amplitudes. Furthermore, it can be shown that, to obtain $\sigma_8 = 0.83$ within our P_ℓ-only analysis, unconventional values of the bias parameters are required, such as $b_2 \approx -2$, which are generally ruled out when the bispectrum is also included. In contrast, the bias parameters associated with our best-fit σ_8 value are generally consistent with the expected halo bias relations discussed in Sec. VI D.

A wide variety of new physics models have been proposed to alleviate the so-called S_8-tension, including via decaying dark matter, modified gravity, interacting dark energy and sterile neutrinos [e.g., [99–103]] (see [104] for a recent review). For most of these models, one would expect a suppression of power at large k, beyond the characteristic scale of the phenomenon. A typical example is the neutrino free-streaming scale $k_{\rm fs} \approx 0.1h$ Mpc^{-1} for $m_\nu \approx 0.1$ eV [105]. Obtaining a model capable of changing only the large-scale quadrupole is a more difficult feat, and may require exotic physics. For instance, the presence of this large-scale discrepancy prohibits the σ_8 difference between BOSS galaxies and the *Planck* CMB being fit by a massive neutrino [106].

An alternative explanation is that there are systematics in our modeling. Given the results of Fig. 8, it seems unlikely that omitted higher-order effects could generate such a shift: σ_8 is primarily set by large scales, whose character is well described by linear physics. One possibility is that selection effects could influence the σ_8 posterior. These arise from anisotropic assembly biases, which violate the symmetry arguments used to construct the bias expansion, with the effect of modifying the large-scale quadrupole [107]. Estimates of the magnitude of this effect range from close to zero [108] to highly significant [109], suggesting the need for further study. Given that our S_8 results are consistent with those from weak lensing probes (which do not have access to redshift-space information), it seems likely that such selection effects do not significantly affect the σ_8 constraints found herein BOSS data. The combination of the above results promote the conclusion that this discrepancy arises simply due to noise fluctuations.

D. Testing bias relations

Galaxy bias parameters are a key part of any perturbative model, yet they enter the power spectrum in a degenerate manner that makes their individual determination difficult (with the exception of linear bias). As a result, previous constraints on the quadratic and tidal biases, b_2, and $b_{\mathcal{G}_2}$ were prior-dominated [e.g., [18]]. In contrast, b_2 and $b_{\mathcal{G}_2}$ appear in the tree-level bispectrum model accompanied by different shapes, allowing them to be directly constrained from data [47]. For dark-matter halos, there are well-known relations between bias parameters [110–115]; the inclusion of bispectrum information allows one to study whether these hold also for observed galaxies.

Marginalized constraints on the galaxy bias parameters for the four BOSS data chunks are given in Table VI & VII

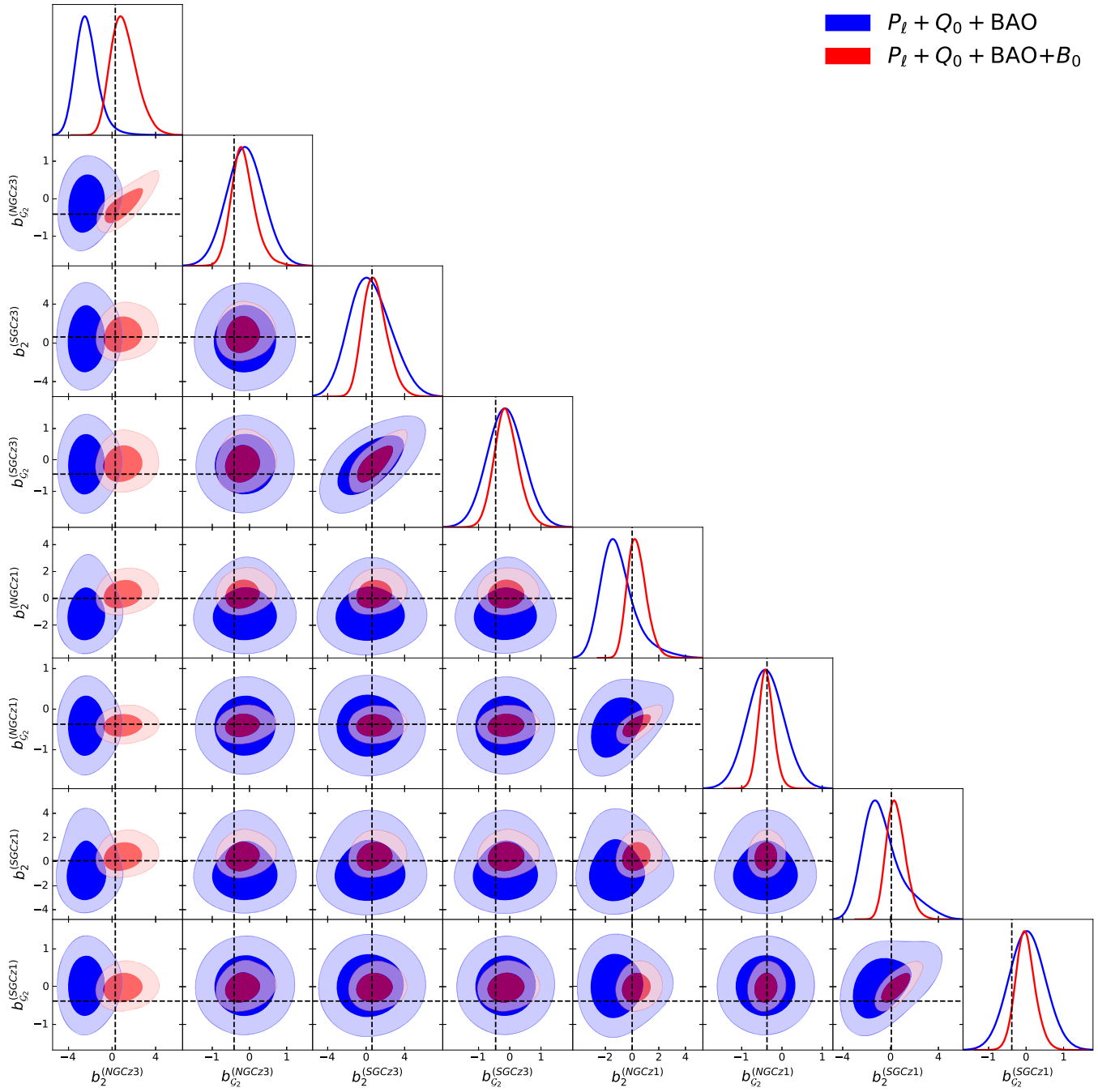

FIG. 9. Quadratic bias parameters from an analysis of the BOSS DR12 power spectrum (blue, including the real-space proxy and BAO parameters) and power spectrum plus bispectrum (right), without imposing restrictive priors. Vertical and horizontal lines mark the predictions of the dark matter halo bias relations for the optimal values of b_1 for each sample, using the formalisms described in the main text. The associated marginalized constraints are shown in Table V. Notably, the large-scale bispectrum significantly sharpens constraints on the second-order biases.

from the power spectrum and bispectrum, optionally including the *Planck* prior on n_s. The inclusion of the bispectrum sharpens second-order bias parameters by up to 30%, with a much greater improvement seen than for the cosmological parameters. In the particular degeneracy direction $b_{\mathcal{G}_2} - b_2/2.3$, the bispectrum narrows the posterior by a factor of two. In reality, this comparison underestimates the utility of the bispectrum since, in its absence, the bias parameter constraints are dominated by restrictive physical priors. If these are not imposed, the posterior widths of the second-order biases are much larger [cf. [18]]. This implies that the actual improvement from the bispectrum can be significantly larger, as found in [47].

TABLE V. Posterior values for the linear and quadratic bias parameters extracted from a power spectrum (left) or power spectrum plus bispectrum (right) analysis without restrictive priors on b_2 and $b_{\mathcal{G}_2}$. The superscripts on bias parameters indicate the sample, in the order NGC z3, SGC z3, NGC z1, SGC z1. The corresponding two-dimensional posterior is shown in Fig. 9.

	$P_\ell + Q_0 + \mathrm{BAO}$				$P_\ell + Q_0 + \mathrm{BAO} + B_0$			
Parameter	Best-fit	mean $\pm\,\sigma$	95% lower	95% upper	Best-fit	mean $\pm\,\sigma$	95% lower	95% upper
$b_1^{(1)}$	2.12	$2.21^{+0.15}_{-0.16}$	1.90	2.52	2.26	$2.45^{+0.15}_{-0.14}$	2.15	2.73
$b_2^{(1)}$	−2.64	$-2.32^{+0.74}_{-1.20}$	−4.37	−0.134	0.273	$1.10^{+1.00}_{-1.40}$	−1.17	3.66
$b_{\mathcal{G}_2}^{(1)}$	−0.106	$-0.12^{+0.44}_{-0.48}$	−1.03	0.808	−0.362	$-0.16^{+0.27}_{-0.36}$	−0.806	0.545
$b_1^{(2)}$	2.34	$2.40^{+0.16}_{-0.16}$	2.09	2.71	2.41	$2.58^{+0.15}_{-0.15}$	2.28	2.88
$b_2^{(2)}$	−0.834	$0.42^{+1.6}_{-2.6}$	−3.13	4.55	0.341	$0.93^{+1.1}_{-1.4}$	−1.49	3.55
$b_{\mathcal{G}_2}^{(2)}$	−0.711	$-0.135^{+0.53}_{-0.57}$	−1.20	0.976	−0.362	$-0.161^{+0.27}_{-0.36}$	−0.806	0.545
$b_1^{(3)}$	2.04	$2.11^{+0.14}_{-0.15}$	1.83	2.40	2.13	$2.30^{+0.13}_{-0.13}$	2.03	2.57
$b_2^{(3)}$	−1.12	$-1.07^{+0.71}_{-1.50}$	−3.33	1.83	−0.024	$0.375^{+0.62}_{-0.82}$	−1.03	1.88
$b_{\mathcal{G}_2}^{(3)}$	−0.386	$-0.409^{+0.4}_{-0.42}$	−1.24	0.443	−0.403	$-0.394^{+0.18}_{-0.20}$	−0.788	0.0072
$b_1^{(4)}$	2.10	$2.15^{+0.14}_{-0.15}$	1.86	2.44	2.16	$2.34^{+0.14}_{-0.14}$	2.06	2.61
$b_2^{(4)}$	−1.86	$-0.689^{+0.79}_{-2.00}$	−3.33	3.09	0.124	$0.478^{+0.70}_{-0.92}$	−1.10	2.21
$b_{\mathcal{G}_2}^{(4)}$	−0.238	$0.0305^{+0.44}_{-0.47}$	−0.879	0.952	−0.203	$-0.014^{+0.25}_{-0.29}$	−0.556	0.550

To explore this, we have rerun our fixed-n_s analysis without restrictive priors on b_2 and $b_{\mathcal{G}_2}$, changing them to flat priors with infinite support. The corresponding constraints are shown in Fig. 9 and in Table. V. Dashed lines in Fig. 9 indicate the predictions based on the dark matter halo bias relations, as above. In the absence of the bispectrum dataset, we find highly non-Gaussian posteriors, with b_2 constraints shifted toward large negative values for almost all data chunks. This behavior suggests that the posteriors are not dominated by the data. Indeed, without the bispectrum there are many unbroken degeneracies between the biases and other nuisance parameters, making b_2 and $b_{\mathcal{G}_2}$ quite sensitive to the choice of priors. When the bispectrum is included, the posterior widths shrink dramatically in all cases, and the distribution becomes closer to Gaussian. For the NGCz3 chunk we find that the power spectrum results are somewhat biased with respect to the dark matter coevolution prediction; this disappears when the bispectrum is included, indicating that it is a statistical fluctuation.

In Fig. 10 we plot the measured quadratic and tidal biases as a function of the linear bias, b_1, and compare this to a fit for $b_2(b_1)$ from dark matter halos [113], and the popular Lagrangian local-in-matter-density (LLIMD) prediction for

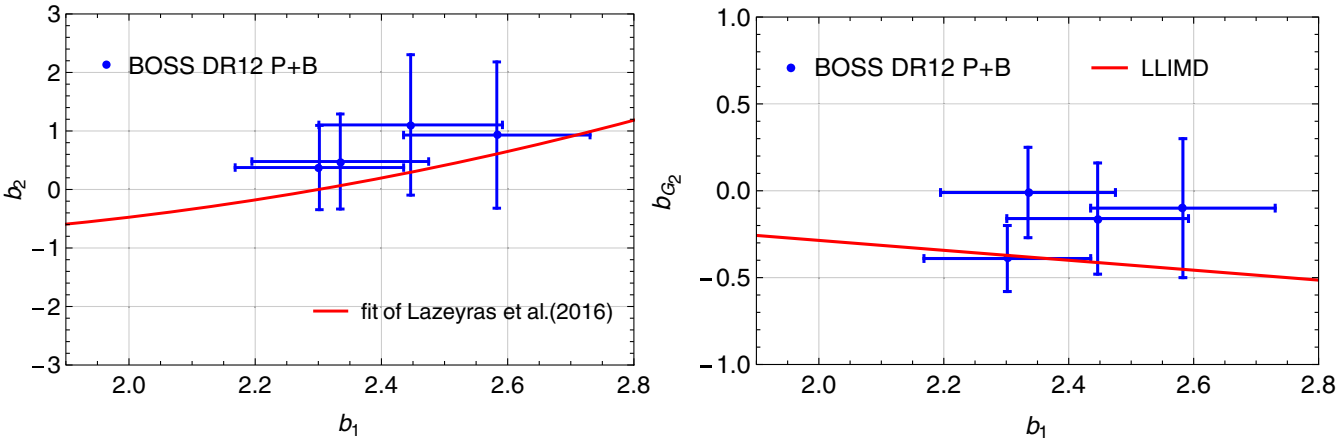

FIG. 10. Linear, quadratic, and tidal bias parameters extracted from the analysis of BOSS DR12 power spectrum and bispectrum data, across two redshift slices and two sky regions. Data-points are shown in blue, while the red curves give predictions for the dark-matter bias relations, from [113,111] for b_2 and $b_{\mathcal{G}_2}$ respectively. Note that in our convention $b_2 = b_2^{\mathrm{ref.}\,[113]} + \frac{4}{3} b_{\mathcal{G}_2}$. We find no evidence that galaxy bias parameters obey different relations to those of dark matter.

$b_{\mathcal{G}_2}(b_1)$. At the current level of precision, we do not detect any significant deviations, thus our results are consistent with the hypothesis that galaxy biases follow dark matter trends. Although some deviations have been found in HOD-enhanced N-body simulations [42,47,112] and hydrodynamic simulations [116], these are too small to detect in BOSS data, though this will likely change with the advent of DESI and Euclid. This also functions as an important consistency test: if the inclusion of the bispectrum had led to strong deviations from the dark matter relations, this would suggest that the bispectrum preferred very different bias parameters to those of the (well-tested) power spectrum. A generic prediction of perturbative models is that the power spectrum and bispectrum depend on the same set of biases, thus this would have indicated that the model was overfitting the data.

VII. SUMMARY AND CONCLUSIONS

In this work, we have presented a full analysis of the BOSS DR12 dataset, utilizing the power spectrum multipoles [18], the real-space power spectrum proxy [78], BAO parameters obtained from the reconstructed power spectra [22] and the bispectrum monopole. Unlike previous analyses, we have measured both the power spectrum and bispectrum using window-free estimators [53,54], which allow them to be straightforwardly compared to theory, with no need for expensive convolution integrals. This enables the bispectrum to be analyzed in reasonable computational time without resorting to systematic-inducing approximations or large-scale cuts [e.g., [7]]. The above work represents the first self-consistent analysis of the power spectrum and bispectrum, obtained using a robust theoretical model based on the effective field theory of large scale structure [47].

By comparison with high-fidelity mock catalogs we have demonstrated the pipeline to be highly robust, and have used this to place the sharpest ever constraints on ΛCDM parameters from a full-shape analysis of BOSS DR12 and a BBN prior on the baryon density. In particular, we find H_0 constraints consistent with previous studies, somewhat below those of SH0ES, and obtain a $<5\%$ constraint on σ_8, equal to $0.722^{+0.032}_{-0.036}$ from the complete analysis with a *Planck* prior on n_s. The inclusion of the bispectrum is found to significantly sharpen constraints on higher-order bias parameters, such as those controlling tidal physics, and leads to a $\approx 13\%$ reduction in the σ_8 error bar, even with our highly conservative analysis choices. If one accepts a slightly larger systematic error budget, or reduces the physical priors on bias parameters, the bispectrum's utility will grow further.

Overall, our results are consistent with those of *Planck* at 95% confidence level [73], but also broadly support the trend for lower S_8 measurements seen in weak lensing datasets [e.g., [95]], with $S_8 = 0.751 \pm 0.039$ found herein. However, we show that our constraint is driven by the large-scale quadrupole amplitude (with $k < 0.1h$ Mpc^{-1}), which disfavors simplistic new physics explanations for the S_8 discrepancy. We have additionally compared our power spectrum results to standard windowed analyses, and those of other groups, and generally find good agreement.

It is interesting to compare the above conclusions to those of simplified power spectrum and bispectrum forecasts [38,117–119]. Perhaps the most relevant is that of [118], which performed a full MCMC forecast for the Euclid spectroscopic survey, utilizing a theoretical model based on perturbation theory (but without calibration to simulations). The former work suggested that inclusion of the tree-level bispectrum monopole would lead to significant improvements on a range of ΛCDM parameters (as well as the neutrino mass), while here we find appreciable changes only in σ_8. In part, this is caused by the difference in galaxy sample. [118] focused on the Euclid or DESI-like emission line galaxies (ELGs), while we here consider only the BOSS luminous red galaxies (LRGs), which violate many of [118]'s assumptions. For instance, preliminary analyses of the ELG power spectrum suggest that this sample has a weak fingers-of-God signature [120], closer to that assumed in [118]. This directly impacts both the theoretical model and the assumed systematic error kernels, which can have a strong impact on the parameter inferences [e.g., [121]]. In contrast, LRGs exhibit strong fingers-of-God (velocity dispersion) effects, implying that the perturbative approximations break down at larger scales, limiting our k-range. Furthermore, the analysis of [118] ignored a number of physical effects such as scale-dependent stochasticity; it is unclear whether these will be important for the DESI ELG sample, given that they appear to be present in the LRG sample [47,60,122]. All in all, our work does not invalidate the results of the previous forecast, but it remains to be seen whether their assumptions will be valid when analyzing the upcoming ELG samples.

This work has demonstrated that robust power spectrum and bispectrum analyses are possible for current datasets, and will open the door to a number of future analyses, both extending the above scope, and testing new models of physics. Possibilities include:

(i) A search for signatures of non-ΛCDM physics. In particular, we can obtain constraints on the neutrino mass using the above framework, sharpen bounds on early dark energy [e.g., [24,123]], and place constraints on primordial non-Gaussianity (PNG). The latter is a particular use-case for the bispectrum: while local-type PNG can be probed in the galaxy power spectrum [e.g., [124]], features such as equilateral PNG can only be probed with higher-order statistics [125–127]. Such extensions will be discussed in future work [128].

(ii) Extension to the anisotropic bispectrum multipoles, B_ℓ (or spherical harmonics, $B_{\ell m}$), analogous to the power spectrum multipoles P_ℓ [129–131]. Such

quantities can be measured using a simple extension of the estimators discussed in Sec. III, and modeled simply by integrating the perturbation theory of Sec. IV against a Legendre polynomial (or spherical harmonic). This will likely enhance the cosmological utility of the bispectrum at fixed $k_{\rm max}$, and reduce any systematics arising from anisotropy of the bispectrum window function.

(iii) Implementation of a real-space bispectrum estimator, analogous to our Q_0 statistic [78] for the power spectrum. This would eliminate the necessity to model stochastic velocities, and increase the range of scales over which the bispectrum could be robustly modeled. An additional option would be to use a theoretical error model [e.g., [132]] to smooth over poorly scales, such that we can extract well-understood oscillatory information in the bispectrum up to high k (cf. [22] for reconstructed power spectra). This information is highly degenerate with that of the BAO parameters however.

(iv) Development of a one-loop model for the galaxy bispectrum, and a more complete treatment of fingers-of-God [e.g., [133]], allowing a larger k-reach in both real- and redshift-space. As shown in [47], redshift-space effects are a limiting factor in our current modeling, and forces us to use lower $k_{\rm max}$ than possible in real-space. Alternatively, we may consider map-level fingers-of-God compression [e.g., [122,134,135]], reducing the amplitude of the effect in the measured statistics.

(v) Compression of the dataset to reduce its dimensionality. This will be of use if narrower k-bins are used, or a larger $k_{\rm max}$, and will help reduce the noise penalty from using a finite number of mocks to derive Gaussian covariance matrices (cf. VI B 2). This may proceed via a generic linear approach [e.g., [89]], or a bispectrum specific framework [50,51,136,137], and the resulting coefficients can likely be estimated directly from the data [54].

In addition, the current methodology can be reapplied to upcoming datasets such as that from DESI and Euclid. Given that the estimators are publicly available, this can be performed with relative ease, especially given that the theoretical model and window-free implementations have already been tested on survey volumes larger than that of the full DESI sample (cf. [47] and Sec. V). Upcoming surveys will include multiple different galaxy samples: of particular interest are the emission line galaxy samples, since they are expected to have a lower contribution from stochastic velocities [120]. This reduces the fingers-of-God effect, enabling smaller scales to be modeled, and thus obtain a greater volume of information from the bispectrum.

As the data volume increases, it will become increasingly important to understand systematics of the data and analysis pipeline. In particular, an important part of any DESI analysis will be a rigorous study of observational effects, such as those arising from sky calibration and poorly known redshift distributions. Given that our analyses include information from a broader range of scales than traditional methods, we are more susceptible to such errors. Assuming that these phenomena can be controlled, we may proceed to perform analysis of upcoming data with higher-order statistics, and thus reap the corresponding rewards.

ACKNOWLEDGMENTS

We are indebted to Giovanni Cabass, Marko Simonovic, and Matias Zaldarriaga for a wealth of insightful discussions. We are additionally grateful to Kazuyuki Akitsu, Shi-Fan Chen, Simone Ferraro, Yosuke Kobayashi, Pat McDonald, Takahiro Nishimichi, David Spergel, Masahiro Takada and Martin White for useful feedback, and the anonymous referee for a insightful comments. O. H. E. P. thanks the Simons Foundation for additional support. The work of M. M. I. has been supported by NASA through the NASA Hubble Fellowship Grant No. HST-HF2-51483.001-A awarded by the Space Telescope Science Institute, which is operated by the Association of Universities for Research in Astronomy, Incorporated, under NASA contract No. NAS5-26555. M. M. I. is an Einstein Fellow. The authors acknowledge that the work reported in this paper was substantially performed using the Research Computing resources at Princeton University which is a consortium of groups led by the Princeton Institute for Computational Science and Engineering (PICSciE) and the Office of Information Technology's Research Computing Division. Funding for SDSS-III has been provided by the Alfred P. Sloan Foundation, the Participating Institutions, the National Science Foundation, and the U.S. Department of Energy Office of Science. The SDSS-III web site is [138]. SDSS-III is managed by the Astrophysical Research Consortium for the Participating Institutions of the SDSS-III Collaboration including the University of Arizona, the Brazilian Participation Group, Brookhaven National Laboratory, Carnegie Mellon University, University of Florida, the French Participation Group, the German Participation Group, Harvard University, the Instituto de Astrofisica de Canarias, the Michigan State/Notre Dame/JINA Participation Group, Johns Hopkins University, Lawrence Berkeley National Laboratory, Max Planck Institute for Astrophysics, Max Planck Institute for Extraterrestrial Physics, New Mexico State University, New York University, Ohio State University, Pennsylvania State University, University of Portsmouth, Princeton University, the Spanish Participation Group, University of Tokyo, University of Utah, Vanderbilt University, University of Virginia, University of Washington, and Yale University. The massive production of all MultiDark-Patchy mocks for the BOSS Final Data Release has been performed at the BSC Marenostrum supercomputer, the Hydra cluster at the Instituto de Fısica Teorica UAM/CSIC, and NERSC at the

Lawrence Berkeley National Laboratory. We acknowledge support from the Spanish MICINNs Consolider-Ingenio 2010 Programme under grant No. MultiDark CSD2009-00064, MINECO Centro de Excelencia Severo Ochoa Programme under Grants No. SEV- 2012-0249, and No. AYA2014-60641-C2-1-P. The MultiDark-Patchy mocks was an effort led from the IFT UAM-CSIC by F. Prada's group (C.-H. Chuang, S. Rodriguez-Torres and C. Scoccola) in collaboration with C. Zhao (Tsinghua U.), F.-S. Kitaura (AIP), A. Klypin (NMSU), G. Yepes (UAM), and the BOSS galaxy clustering working group.

APPENDIX: FULL PARAMETER CONSTRAINTS

In this Appendix, we give the full marginalized posteriors for all cosmological and noncosmological parameters sampled within the MCMC likelihoods, using the full power spectrum likelihood (including BAO and Q_0 datasets), and the power spectrum plus bispectrum joint likelihood. Parameters entering the model linearly (such as $P_{\rm shot}$) are marginalized over analytically, and thus excluded. Results are shown in Tables VI and VII, and in Figs. 11 and 12, with the latter set including a *Planck* prior on n_s.

TABLE VI. Full parameter constraints from the ΛCDM analysis of BOSS DR12 data using the power spectrum datasets ($P_\ell + Q_0 + \mathrm{BAO}$, left) and including the bispectrum ($P_\ell + Q_0 + \mathrm{BAO}$, right). We give the best-fit values, the mean, 68%, and 95% confidence level results in each case, and show the derived parameters in the bottom rows. The superscripts on bias parameters indicate the sample, in the order NGC z3, SGC z3, NGC z1, SGC z1. The associated two-dimensional posteriors are shown in Fig. 11. Corresponding results with a *Planck* prior on n_s are shown in Table VII.

	$P_\ell + Q_0 + \mathrm{BAO}$				$P_\ell + Q_0 + \mathrm{BAO} + B_0$			
Parameter	Best-fit	Mean $\pm\,\sigma$	95% lower	95% upper	Best-fit	Mean $\pm\,\sigma$	95% lower	95% upper
$\omega_{\rm cdm}$	0.1322	$0.1366^{+0.011}_{-0.013}$	0.1139	0.1601	0.1378	$0.1405^{+0.011}_{-0.013}$	0.1175	0.164
h	0.6903	$0.6931^{+0.011}_{-0.012}$	0.6688	0.717	0.6944	$0.6957^{+0.011}_{-0.013}$	0.6719	0.7203
$\ln(10^{10}A_s)$	2.729	$2.657^{+0.14}_{-0.15}$	2.366	2.951	2.603	$2.599^{+0.13}_{-0.14}$	2.339	2.871
n_s	0.891	$0.8741^{+0.067}_{-0.064}$	0.7431	1.006	0.8698	$0.8697^{+0.067}_{-0.064}$	0.7391	1.003
$b_1^{(1)}$	2.263	$2.331^{+0.15}_{-0.15}$	2.031	2.644	2.406	$2.411^{+0.13}_{-0.13}$	2.154	2.67
$b_2^{(1)}$	−0.9937	$-1.094^{+0.84}_{-1}$	−2.881	0.8157	0.1082	$0.3584^{+0.71}_{-0.78}$	−1.124	1.881
$b_{\mathcal{G}_2}^{(1)}$	−0.2681	$-0.1914^{+0.43}_{-0.43}$	−1.047	0.6657	−0.4004	$-0.3368^{+0.37}_{-0.37}$	−1.089	0.3987
$b_1^{(2)}$	2.411	$2.483^{+0.15}_{-0.15}$	2.186	2.786	2.564	$2.539^{+0.13}_{-0.13}$	2.278	2.797
$b_2^{(2)}$	−0.3943	$-0.004331^{+0.91}_{-0.93}$	−1.812	1.853	0.7517	$0.3415^{+0.75}_{-0.8}$	−1.183	1.901
$b_{\mathcal{G}_2}^{(2)}$	−0.6292	$-0.2781^{+0.43}_{-0.44}$	−1.144	0.5858	−0.3779	$-0.2246^{+0.41}_{-0.41}$	−1.045	0.5843
$b_1^{(3)}$	2.15	$2.211^{+0.14}_{-0.14}$	1.932	2.489	2.239	$2.269^{+0.12}_{-0.12}$	2.031	2.504
$b_2^{(3)}$	−0.3785	$-0.509^{+0.79}_{-0.97}$	−2.189	1.301	0.2004	$0.2082^{+0.59}_{-0.64}$	−1.018	1.438
$b_{\mathcal{G}_2}^{(3)}$	−0.3157	$-0.3832^{+0.37}_{-0.37}$	−1.114	0.3501	−0.3576	$-0.4074^{+0.32}_{-0.32}$	−1.044	0.2281
$b_1^{(4)}$	2.176	$2.248^{+0.14}_{-0.14}$	1.961	2.532	2.307	$2.303^{+0.12}_{-0.12}$	2.056	2.552
$b_2^{(4)}$	−0.2319	$-0.3743^{+0.87}_{-1}$	−2.178	1.523	0.042	$0.006909^{+0.65}_{-0.72}$	−1.346	1.381
$b_{\mathcal{G}_2}^{(4)}$	−0.05649	$-0.002389^{+0.38}_{-0.4}$	−0.7803	0.7901	−0.219	$-0.2876^{+0.37}_{-0.37}$	−1.018	0.4428
Ω_m	0.327	$0.3326^{+0.016}_{-0.018}$	0.2998	0.366	0.3342	$0.3381^{+0.016}_{-0.017}$	0.3056	0.3703
H_0	69.03	$69.31^{+1.1}_{-1.2}$	66.88	71.7	69.44	$69.57^{+1.1}_{-1.3}$	67.19	72.03
σ_8	0.7158	$0.7011^{+0.04}_{-0.045}$	0.6169	0.7876	0.6856	$0.6917^{+0.035}_{-0.041}$	0.6165	0.7698

TABLE VII. As Table VI, but including a *Planck* prior on the spectral slope n_s. The associated two-dimensional posteriors are shown in Fig. 12.

	$P_\ell + Q_0 + \mathrm{BAO}$				$P_\ell + Q_0 + \mathrm{BAO} + B_0$			
Parameter	Best-fit	Mean $\pm \sigma$	95% lower	95% upper	Best-fit	Mean $\pm \sigma$	95% lower	95% upper
$\omega_{\rm cdm}$	0.1218	$0.1227^{+0.0053}_{-0.0059}$	0.1118	0.134	0.1242	$0.1262^{+0.0053}_{-0.0059}$	0.1152	0.1374
h	0.6778	$0.6811^{+0.0083}_{-0.0089}$	0.6641	0.6981	0.6809	$0.6831^{+0.0083}_{-0.0086}$	0.6665	0.7002
$\ln(10^{10}A_s)$	2.863	$2.795^{+0.11}_{-0.12}$	2.572	3.022	2.771	$2.741^{+0.096}_{-0.098}$	2.548	2.935
$b_1^{(1)}$	2.217	$2.288^{+0.15}_{-0.15}$	1.993	2.579	2.335	$2.365^{+0.12}_{-0.13}$	2.115	2.619
$b_2^{(1)}$	−1.033	$-1.045^{+0.81}_{-0.96}$	−2.769	0.74	0.4944	$0.4867^{+0.69}_{-0.78}$	−0.9661	1.976
$b_{\mathcal{G}_2}^{(1)}$	−0.03938	$-0.01572^{+0.39}_{-0.41}$	−0.8159	0.7855	−0.08666	$-0.1783^{+0.34}_{-0.34}$	−0.8567	0.5097
$b_1^{(2)}$	2.387	$2.449^{+0.15}_{-0.14}$	2.156	2.744	2.471	$2.502^{+0.13}_{-0.13}$	2.243	2.766
$b_2^{(2)}$	−0.4042	$0.01267^{+0.88}_{-0.98}$	−1.793	1.868	0.5985	$0.3589^{+0.74}_{-0.79}$	−1.16	1.886
$b_{\mathcal{G}_2}^{(2)}$	−0.3214	$-0.1954^{+0.42}_{-0.42}$	−1.03	0.6524	−0.2001	$-0.1392^{+0.39}_{-0.4}$	−0.9232	0.6532
$b_1^{(3)}$	2.093	$2.172^{+0.13}_{-0.13}$	1.9	2.44	2.179	$2.227^{+0.11}_{-0.12}$	1.996	2.459
$b_2^{(3)}$	−0.5351	$-0.4924^{+0.76}_{-0.96}$	−2.168	1.276	0.2993	$0.2286^{+0.58}_{-0.64}$	−0.9688	1.469
$b_{\mathcal{G}_2}^{(3)}$	−0.4988	$-0.3075^{+0.36}_{-0.37}$	−1.026	0.4293	−0.335	$-0.3311^{+0.3}_{-0.32}$	−0.9516	0.2952
$b_1^{(4)}$	2.141	$2.209^{+0.14}_{-0.14}$	1.933	2.489	2.207	$2.264^{+0.12}_{-0.13}$	2.022	2.509
$b_2^{(4)}$	−0.8938	$-0.358^{+0.81}_{-1}$	−2.106	1.486	−0.4185	$0.007424^{+0.63}_{-0.71}$	−1.293	1.349
$b_{\mathcal{G}_2}^{(4)}$	0.02433	$0.05553^{+0.37}_{-0.39}$	−0.7031	0.8315	−0.3927	$-0.2495^{+0.35}_{-0.36}$	−0.9517	0.4648
Ω_m	0.3153	$0.3142^{+0.0095}_{-0.01}$	0.2949	0.3338	0.3176	$0.3197^{+0.0095}_{-0.01}$	0.3005	0.3393
H_0	67.78	$68.11^{+0.83}_{-0.89}$	66.41	69.81	68.09	$68.31^{+0.83}_{-0.86}$	66.65	70.02
σ_8	0.7491	$0.7286^{+0.036}_{-0.042}$	0.6511	0.8088	0.7248	$0.722^{+0.032}_{-0.036}$	0.6536	0.7915

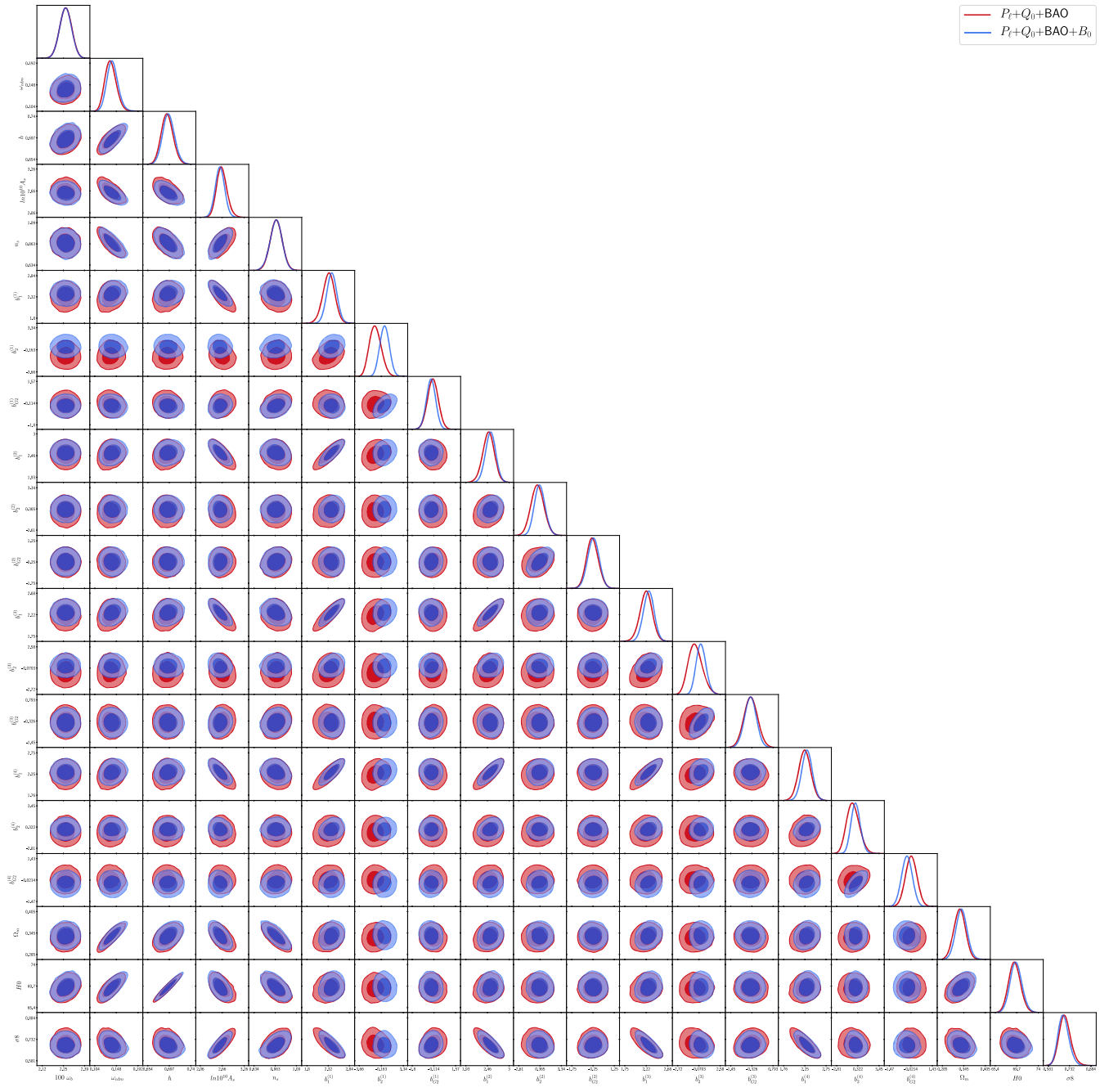

FIG. 11. Full posterior plot of the cosmological and nuisance parameter posteriors measured from the BOSS DR12 data, with a BBN prior on the ω_b. We show results for both the full power spectrum ($P_\ell + Q_0 + \mathrm{BAO}$) and the joint analysis of power spectrum and bispectrum. The corresponding parameter constraints are given in Table VI.

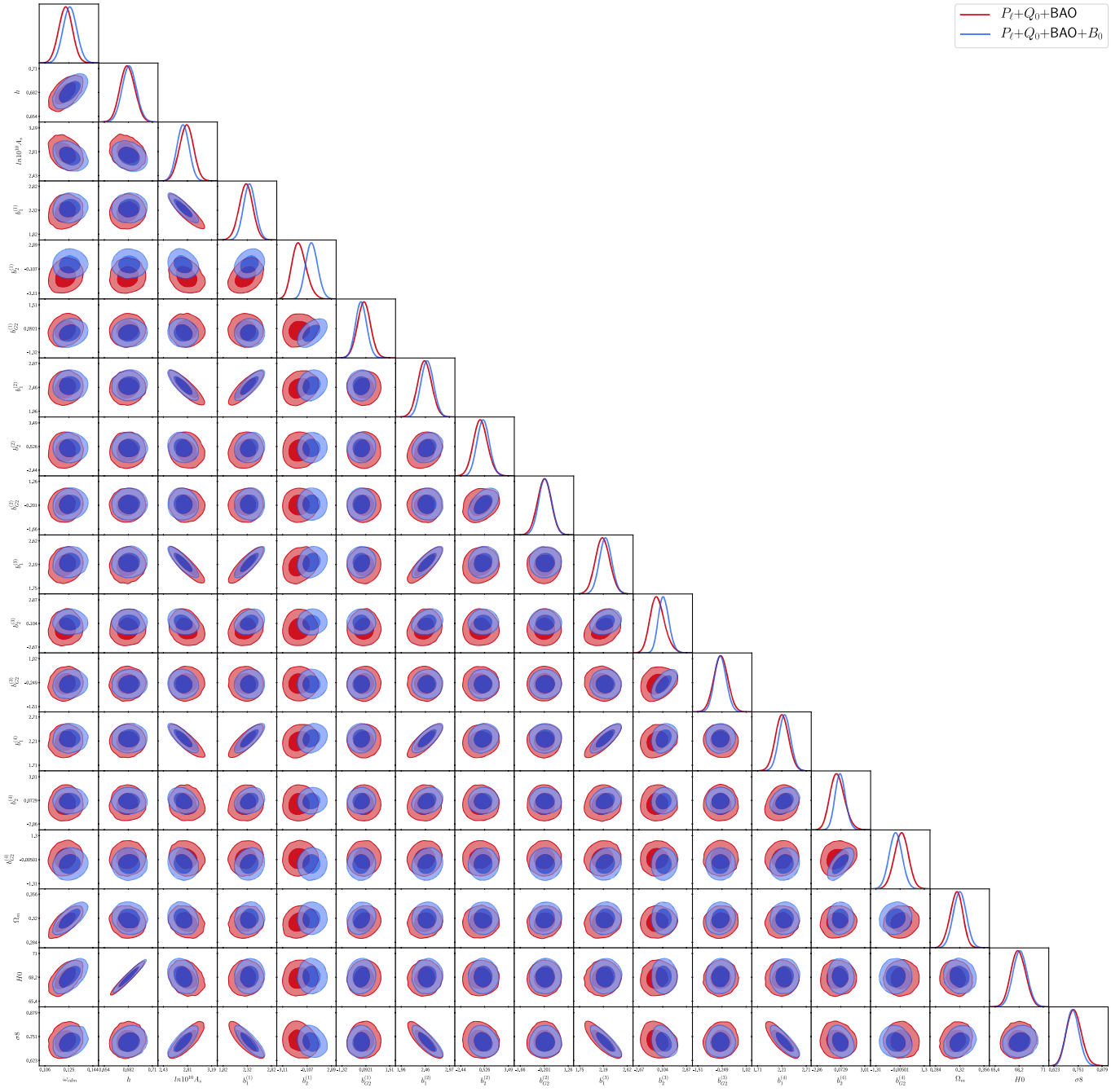

FIG. 12. As Fig. 11, but including a *Planck* prior on n_s. The corresponding parameter constraints are given in Table VII.

[1] A. A. Starobinsky, Dynamics of phase transition in the new inflationary universe scenario and generation of perturbations, Phys. Lett. **117B**, 175 (1982).

[2] A. D. Linde, Scalar field fluctuations in the expanding universe and the new inflationary universe scenario, Phys. Lett. **116B**, 335 (1982).

[3] F. Bernardeau, S. Colombi, E. Gaztañaga, and R. Scoccimarro, Large-scale structure of the Universe and cosmological perturbation theory, Phys. Rep. **367**, 1 (2002).

[4] R. Scoccimarro, H. A. Feldman, J. N. Fry, and J. A. Frieman, The Bispectrum of IRAS redshift catalogs, Astrophys. J. **546**, 652 (2001).

[5] E. Sefusatti, M. Crocce, S. Pueblas, and R. Scoccimarro, Cosmology and the bispectrum, Phys. Rev. D **74**, 023522 (2006).
[6] H. Gil-Marín, J. Noreña, L. Verde, W. J. Percival, C. Wagner, M. Manera, and D. P. Schneider, The power spectrum and bispectrum of SDSS DR11 BOSS galaxies—I. Bias and gravity, Mon. Not. R. Astron. Soc. **451**, 539 (2015).
[7] H. Gil-Marín, W. J. Percival, L. Verde, J. R. Brownstein, C.-H. Chuang, F.-S. Kitaura , S. A. Rodríguez-Torres, and M. D. Olmstead, The clustering of galaxies in the SDSS-III Baryon Oscillation Spectroscopic Survey: RSD measurement from the power spectrum and bispectrum of the DR12 BOSS galaxies, Mon. Not. R. Astron. Soc. **465**, 1757 (2017).
[8] F. Beutler and P. McDonald, Unified galaxy power spectrum measurements from 6dFGS, BOSS, and eBOSS, J. Cosmol. Astropart. Phys. 11 (2021) 031.
[9] H. Gil-Marín, J. E. Bautista, R. Paviot, M. Vargas-Magaña, S. de la Torre, S. Fromenteau *et al.*, The completed SDSS-IV extended baryon oscillation spectroscopic survey: Measurement of the BAO and growth rate of structure of the luminous red galaxy sample from the anisotropic power spectrum between redshifts 0.6 and 1.0, Mon. Not. R. Astron. Soc. **498**, 2492 (2020).
[10] S. Alam, M. Ata, S. Bailey, F. Beutler, D. Bizyaev, J. A. Blazek *et al.*, The clustering of galaxies in the completed SDSS-III baryon oscillation spectroscopic survey: Cosmological analysis of the DR12 galaxy sample, Mon. Not. R. Astron. Soc. **470**, 2617 (2017).
[11] F. Beutler, H.-J. Seo, A. J. Ross, P. McDonald, S. Saito, A. S. Bolton *et al.*, The clustering of galaxies in the completed SDSS-III baryon oscillation spectroscopic survey: Baryon acoustic oscillations in the fourier space, Mon. Not. R. Astron. Soc. **464**, 3409 (2017).
[12] F. Beutler, H.-J. Seo, S. Saito, C.-H. Chuang, A. J. Cuesta, D. J. Eisenstein *et al.*, The clustering of galaxies in the completed SDSS-III baryon oscillation spectroscopic survey: Anisotropic galaxy clustering in Fourier space, Mon. Not. R. Astron. Soc. **466**, 2242 (2017).
[13] D. J. Eisenstein, H.-J. Seo, E. Sirko, and D. N. Spergel, Improving cosmological distance measurements by reconstruction of the baryon acoustic peak, Astrophys. J. **664**, 675 (2007).
[14] Y. Noh, M. White, and N. Padmanabhan, Reconstructing baryon oscillations, Phys. Rev. D **80**, 123501 (2009).
[15] N. Padmanabhan, X. Xu, D. J. Eisenstein, R. Scalzo, A. J. Cuesta, K. T. Mehta, and E. Kazin, A 2 per cent distance to $z = 0.35$ by reconstructing baryon acoustic oscillations—I. Methods and application to the Sloan Digital Sky Survey, Mon. Not. R. Astron. Soc. **427**, 2132 (2012).
[16] M. Schmittfull, Y. Feng, F. Beutler, B. Sherwin, and M. Y. Chu, Eulerian BAO reconstructions and N-point statistics, Phys. Rev. D **92**, 123522 (2015).
[17] D. W. Pearson and L. Samushia, A detection of the baryon acoustic oscillation features in the SDSS BOSS DR12 galaxy bispectrum, Mon. Not. R. Astron. Soc. **478**, 4500 (2018).
[18] M. M. Ivanov, M. Simonović, and M. Zaldarriaga, Cosmological parameters from the BOSS galaxy power spectrum, J. Cosmol. Astropart. Phys. 05 (2020) 042.
[19] G. d'Amico, J. Gleyzes, N. Kokron, K. Markovic, L. Senatore, P. Zhang, F. Beutler, and H. Gil-Marín, The cosmological analysis of the SDSS/BOSS data from the effective field theory of large-scale structure, J. Cosmol. Astropart. Phys. 05 (2020) 005.
[20] S.-F. Chen, Z. Vlah, and M. White, A new analysis of the BOSS survey, including full-shape information and post-reconstruction BAO, arXiv:2110.05530.
[21] Y. Kobayashi, T. Nishimichi, M. Takada, and H. Miyatake, Full-shape cosmology analysis of SDSS-III BOSS galaxy power spectrum using emulator-based halo model: A 5% determination of σ_8, arXiv:2110.06969.
[22] O. H. E. Philcox, M. M. Ivanov, M. Simonović, and M. Zaldarriaga, Combining full-shape and BAO analyses of galaxy power spectra: A 1.6% CMB-independent constraint on H_0, J. Cosmol. Astropart. Phys. 05 (2020) 032.
[23] A. Chudaykin, K. Dolgikh, and M. M. Ivanov, Constraints on the curvature of the Universe and dynamical dark energy from the full-shape and BAO data, Phys. Rev. D **103**, 023507 (2021).
[24] M. M. Ivanov, E. McDonough, J. C. Hill, M. Simonović, M. W. Toomey, S. Alexander, and M. Zaldarriaga, Constraining early dark energy with large-scale structure, Phys. Rev. D **102**, 103502 (2020).
[25] G. D'Amico, L. Senatore, P. Zhang, and H. Zheng, The Hubble tension in light of the full-shape analysis of large-scale structure data, J. Cosmol. Astropart. Phys. 05 (2021) 072.
[26] W. L. Xu, J. B. Muñoz, and C. Dvorkin, Cosmological constraints on light (but massive) relics, arXiv:2107.09664.
[27] A. Laguë, J. R. Bond, R. Hložek, K. K. Rogers, D. J. E. Marsh, and D. Grin, Constraining ultralight axions with galaxy surveys, J. Cosmol. Astropart. Phys. 01 (2022) 049.
[28] O. H. E. Philcox, B. D. Sherwin, G. S. Farren, and E. J. Baxter, Determining the Hubble constant without the sound horizon: Measurements from galaxy surveys, Phys. Rev. D **103**, 023538 (2021).
[29] R. Scoccimarro, S. Colombi, J. N. Fry, J. A. Frieman, E. Hivon, and A. Melott, Nonlinear evolution of the bispectrum of cosmological perturbations, Astrophys. J. **496**, 586 (1998).
[30] R. Scoccimarro, H. M. P. Couchman, and J. A. Frieman, The bispectrum as a signature of gravitational instability in redshift space, Astrophys. J. **517**, 531 (1999).
[31] R. Scoccimarro, The bispectrum: From theory to observations, Astrophys. J. **544**, 597 (2000).
[32] R. Scoccimarro and H. M. P. Couchman, A fitting formula for the non-linear evolution of the bispectrum, Mon. Not. R. Astron. Soc. **325**, 1312 (2001).
[33] R. E. Angulo, S. Foreman, M. Schmittfull, and L. Senatore, The one-loop matter bispectrum in the effective field theory of large scale structures, J. Cosmol. Astropart. Phys. 10 (2015) 039.
[34] T. Baldauf, L. Mercolli, M. Mirbabayi, and E. Pajer, The bispectrum in the effective field theory of large scale structure, J. Cosmol. Astropart. Phys. 05 (2015) 007.
[35] F. Kamalinejad and Z. Slepian, A non-degenerate neutrino mass signature in the galaxy bispectrum, arXiv:2011.00899.
[36] D. Gualdi, H. Gil-Marín, and L. Verde, Joint analysis of anisotropic power spectrum, bispectrum and trispectrum: Application to N-body simulations, J. Cosmol. Astropart. Phys. 07 (2021) 008.

[37] C. Hahn and F. Villaescusa-Navarro, Constraining M_ν with the bispectrum. Part II. The information content of the galaxy bispectrum monopole, J. Cosmol. Astropart. Phys. 04 (2021) 029.
[38] N. Agarwal, V. Desjacques, D. Jeong, and F. Schmidt, Information content in the redshift-space galaxy power spectrum and bispectrum, J. Cosmol. Astropart. Phys. 03 (2021) 021.
[39] J. Byun, A. Oddo, C. Porciani, and E. Sefusatti, Towards cosmological constraints from the compressed modal bispectrum: A robust comparison of real-space bispectrum estimators, J. Cosmol. Astropart. Phys. 03 (2021) 105.
[40] A. Eggemeier, R. Scoccimarro, and R. E. Smith, Bias loop corrections to the galaxy bispectrum, Phys. Rev. D **99**, 123514 (2019).
[41] J. Byun, A. Oddo, C. Porciani, and E. Sefusatti, Towards cosmological constraints from the compressed modal bispectrum: A robust comparison of real-space bispectrum estimators, J. Cosmol. Astropart. Phys. 03 (2021) 105.
[42] A. Eggemeier, R. Scoccimarro, R. E. Smith, M. Crocce, A. Pezzotta, and A. G. Sánchez, Testing one-loop galaxy bias: Joint analysis of power spectrum and bispectrum, Phys. Rev. D **103**, 123550 (2021).
[43] A. Oddo, F. Rizzo, E. Sefusatti, C. Porciani, and P. Monaco, Cosmological parameters from the likelihood analysis of the galaxy power spectrum and bispectrum in real space, J. Cosmol. Astropart. Phys. 11 (2021) 038.
[44] K. Osato, T. Nishimichi, A. Taruya, and F. Bernardeau, Implementing spectra response function approaches for fast calculation of power spectra and bispectra, Phys. Rev. D **104**, 103501 (2021).
[45] A. Taruya, T. Nishimichi, and D. Jeong, Grid-based calculations of redshift-space matter fluctuations from perturbation theory: UV sensitivity and convergence at the field level, arXiv:2109.06734.
[46] T. Baldauf, M. Garny, P. Taule, and T. Steele, The two-loop bispectrum of large-scale structure, Phys. Rev. D **104**, 123551 (2021).
[47] M. M. Ivanov, O. H. E. Philcox, T. Nishimichi, M. Simonović, M. Takada, and M. Zaldarriaga, Precision analysis of the redshift-space galaxy bispectrum, arXiv:2110.10161.
[48] J. N. Fry and M. Seldner, Transform analysis of the high-resolution Shane-Wirtanen Catalog—The power spectrum and the bispectrum, Astrophys. J. **259**, 474 (1982).
[49] R. Scoccimarro, H. A. Feldman, J. N. Fry, and J. A. Frieman, The bispectrum of IRAS redshift catalogs, Astrophys. J. **546**, 652 (2001).
[50] D. Gualdi, H. Gil-Marín, R. L. Schuhmann, M. Manera, B. Joachimi, and O. Lahav, Enhancing BOSS bispectrum cosmological constraints with maximal compression, Mon. Not. R. Astron. Soc. **484**, 3713 (2019).
[51] N. S. Sugiyama, S. Saito, F. Beutler, and H.-J. Seo, A complete FFT-based decomposition formalism for the redshift-space bispectrum, Mon. Not. R. Astron. Soc. **484**, 364 (2019).
[52] N. S. Sugiyama, S. Saito, F. Beutler, and H.-J. Seo, Perturbation theory approach to predict the covariance matrices of the galaxy power spectrum and bispectrum in redshift space, Mon. Not. R. Astron. Soc. **497**, 1684 (2020).
[53] O. H. E. Philcox, Cosmology without window functions: Quadratic estimators for the galaxy power spectrum, Phys. Rev. D **103**, 103504 (2021).
[54] O. H. E. Philcox, Cosmology without window functions: Cubic estimators for the galaxy bispectrum, Phys. Rev. D **104**, 123529 (2021).
[55] M. Tegmark, How to measure CMB power spectra without losing information, Phys. Rev. D **55**, 5895 (1997).
[56] M. Tegmark, A. J. S. Hamilton, and Y. Xu, The power spectrum of galaxies in the 2dF 100k redshift survey, Mon. Not. R. Astron. Soc. **335**, 887 (2002).
[57] M. Tegmark, A. J. S. Hamilton, M. A. Strauss, M. S. Vogeley, and A. S. Szalay, Measuring the galaxy power spectrum with future redshift surveys, Astrophys. J. **499**, 555 (1998).
[58] A. J. S. Hamilton, Power spectrum estimation II. Linear maximum likelihood, Lect. Notes Phys. **665**, 433 (2008).
[59] S. Alam, F. D. Albareti, C. Allende Prieto, F. Anders, S. F. Anderson, T. Anderton *et al.*, The eleventh and twelfth data releases of the sloan digital sky survey: Final data from SDSS-III, Astrophys. J. Suppl. Ser. **219**, 12 (2015).
[60] T. Nishimichi, G. D'Amico, M. M. Ivanov, L. Senatore, M. Simonović, M. Takada, M. Zaldarriaga, and P. Zhang, Blinded challenge for precision cosmology with large-scale structure: Results from effective field theory for the redshift-space galaxy power spectrum, Phys. Rev. D **102**, 123541 (2020).
[61] V. Desjacques, D. Jeong, and F. Schmidt, The galaxy power spectrum and bispectrum in redshift space, J. Cosmol. Astropart. Phys. 12 (2018) 035.
[62] D. Blas, M. Garny, M. M. Ivanov, and S. Sibiryakov, Time-sliced perturbation theory for large scale structure I: General formalism, J. Cosmol. Astropart. Phys. 07 (2016) 052.
[63] D. Blas, M. Garny, M. M. Ivanov, and S. Sibiryakov, Time-sliced perturbation theory II: Baryon acoustic oscillations and infrared resummation, J. Cosmol. Astropart. Phys. 07 (2016) 028.
[64] M. M. Ivanov and S. Sibiryakov, Infrared resummation for biased tracers in redshift space, J. Cosmol. Astropart. Phys. 07 (2018) 053.
[65] A. Vasudevan, M. M. Ivanov, S. Sibiryakov, and J. Lesgourgues, Time-sliced perturbation theory with primordial non-Gaussianity and effects of large bulk flows on inflationary oscillating features, J. Cosmol. Astropart. Phys. 09 (2019) 037.
[66] D. Karagiannis, A. Lazanu, M. Liguori, A. Raccanelli, N. Bartolo, and L. Verde, Constraining primordial non-Gaussianity with bispectrum and power spectrum from upcoming optical and radio surveys, Mon. Not. R. Astron. Soc. **478**, 1341 (2018).
[67] D. J. Eisenstein, D. H. Weinberg, E. Agol, H. Aihara, C. Allende Prieto, S. F. Anderson *et al.*, SDSS-III: Massive spectroscopic surveys of the distant universe, the milky way, and extra-solar planetary systems, Astron. J. **142**, 72 (2011).
[68] F.-S. Kitaura, S. Rodríguez-Torres, C.-H. Chuang, C. Zhao, F. Prada, H. Gil-Marín *et al.*, The clustering of galaxies in the SDSS-III baryon oscillation spectroscopic survey: Mock galaxy catalogues for the BOSS

final data release, Mon. Not. R. Astron. Soc. **456**, 4156 (2016).
[69] S. A. Rodríguez-Torres, C.-H. Chuang, F. Prada, H. Guo, A. Klypin, P. Behroozi *et al.*, The clustering of galaxies in the SDSS-III baryon oscillation spectroscopic survey: Modelling the clustering and halo occupation distribution of BOSS CMASS galaxies in the final data release, Mon. Not. R. Astron. Soc. **460**, 1173 (2016).
[70] E. Aver, K. A. Olive, and E. D. Skillman, The effects of He I λ10830 on helium abundance determinations, J. Cosmol. Astropart. Phys. 07 (2015) 011.
[71] R. J. Cooke, M. Pettini, and C. C. Steidel, One percent determination of the primordial deuterium abundance, Astrophys. J. **855**, 102 (2018).
[72] N. Schöneberg, J. Lesgourgues, and D. C. Hooper, The BAO + BBN take on the Hubble tension, J. Cosmol. Astropart. Phys. 10 (2019) 029.
[73] N. Aghanim, Y. Akrami, M. Ashdown, J. Aumont, C. Baccigalupi *et al.* (Planck Collaboration), Planck 2018 results. VI. Cosmological parameters, Astron. Astrophys. **641**, A6 (2020).
[74] H. A. Feldman, N. Kaiser, and J. A. Peacock, Power-spectrum analysis of three-dimensional redshift surveys, Astrophys. J. **426**, 23 (1994).
[75] R. Scoccimarro, Fast estimators for redshift-space clustering, Phys. Rev. D **92**, 083532 (2015).
[76] D. Bianchi, H. Gil-Marín, R. Ruggeri, and W. J. Percival, Measuring line-of-sight-dependent Fourier-space clustering using FFTs, Mon. Not. R. Astron. Soc. **453**, L11 (2015).
[77] K. M. Smith and M. Zaldarriaga, Algorithms for bispectra: forecasting, optimal analysis and simulation, Mon. Not. R. Astron. Soc. **417**, 2 (2011).
[78] M. M. Ivanov, O. H. E. Philcox, M. Simonović, M. Zaldarriaga, T. Nishimichi, and M. Takada, Cosmological constraints without fingers of God, arXiv:2110.00006.
[79] A. J. S. Hamilton and M. Tegmark, The Real space power spectrum of the PSCz survey from 0.01 to 300h Mpc^{-1}, Mon. Not. R. Astron. Soc. **330**, 506 (2002).
[80] R. Scoccimarro, Redshift-space distortions, pairwise velocities and nonlinearities, Phys. Rev. D **70**, 083007 (2004).
[81] A. Chudaykin, M. M. Ivanov, O. H. E. Philcox, and M. Simonović, Nonlinear perturbation theory extension of the Boltzmann code CLASS, Phys. Rev. D **102**, 063533 (2020).
[82] S.-F. Chen, Z. Vlah, and M. White, Consistent modeling of velocity statistics and redshift-space distortions in one-loop perturbation theory, J. Cosmol. Astropart. Phys. 07 (2020) 062.
[83] G. D'Amico, L. Senatore, and P. Zhang, Limits on wCDM from the EFTofLSS with the PyBird code, J. Cosmol. Astropart. Phys. 01 (2021) 006.
[84] C. Alcock and B. Paczynski, An evolution free test for non-zero cosmological constant, Nature (London) **281**, 358 (1979).
[85] J. Hartlap, P. Simon, and P. Schneider, Why your model parameter confidences might be too optimistic. Unbiased estimation of the inverse covariance matrix, Astron. Astrophys. **464**, 399 (2007).
[86] E. Sellentin and A. F. Heavens, Parameter inference with estimated covariance matrices, Mon. Not. R. Astron. Soc. **456**, L132 (2016).
[87] D. Wadekar and R. Scoccimarro, Galaxy power spectrum multipoles covariance in perturbation theory, Phys. Rev. D **102**, 123517 (2020).
[88] M. M. Ivanov, Y. Ali-Haïmoud, and J. Lesgourgues, H0 tension or T0 tension?, Phys. Rev. D **102**, 063515 (2020).
[89] O. H. E. Philcox, M. M. Ivanov, M. Zaldarriaga, M. Simonović, and M. Schmittfull, Fewer mocks and less noise: Reducing the dimensionality of cosmological observables with subspace projections, Phys. Rev. D **103**, 043508 (2021).
[90] T. Brinckmann and J. Lesgourgues, MontePython 3: Boosted MCMC sampler and other features, Phys. Dark Universe **24**, 100260 (2019).
[91] A. G. Riess, S. Casertano, W. Yuan, J. B. Bowers, L. Macri, J. C. Zinn, and D. Scolnic, Cosmic distances calibrated to 1% precision with gaia EDR3 parallaxes and Hubble space telescope photometry of 75 Milky Way cepheids confirm tension with ΛCDM, Astrophys. J. Lett. **908**, L6 (2021).
[92] D. M. Scolnic, D. O. Jones, A. Rest, Y. C. Pan, R. Chornock, R. J. Foley *et al.*, The complete light-curve sample of spectroscopically confirmed SNe Ia from pan-STARRS1 and cosmological constraints from the combined pantheon sample, Astrophys. J. **859**, 101 (2018).
[93] A. de Mattia, V. Ruhlmann-Kleider, A. Raichoor, A. J. Ross, A. Tamone, C. Zhao *et al.*, The completed SDSS-IV extended Baryon Oscillation Spectroscopic Survey: measurement of the BAO and growth rate of structure of the emission line galaxy sample from the anisotropic power spectrum between redshift 0.6 and 1.1, Mon. Not. R. Astron. Soc. **501**, 5616 (2021).
[94] N. Hand, Y. Feng, F. Beutler, Y. Li, C. Modi, U. Seljak, and Z. Slepian, nbodykit: An Open-source, Massively Parallel Toolkit for Large-scale Structure, Astron. J. **156**, 160 (2018).
[95] T. M. C. Abbott, M. Aguena, A. Alarcon, S. Allam, O. Alves *et al.* (DES Collaboration), Dark energy survey year 3 results: Cosmological constraints from galaxy clustering and weak lensing, Phys. Rev. D **105**, 023520 (2022).
[96] A. Krolewski, S. Ferraro, and M. White, Cosmological constraints from unWISE and Planck CMB lensing tomography, J. Cosmol. Astropart. Phys. 12 (2021) 028.
[97] M. White, R. Zhou, J. DeRose, S. Ferraro, S.-F. Chen, N. Kokron *et al.*, Cosmological constraints from the tomographic cross-correlation of DESI Luminous Red Galaxies and Planck CMB lensing, arXiv:2111.09898.
[98] D. Wadekar, M. M. Ivanov, and R. Scoccimarro, Cosmological constraints from BOSS with analytic covariance matrices, Phys. Rev. D **102**, 123521 (2020).
[99] P. A. R. Ade, N. Aghanim, M. Arnaud, M. Ashdown, J. Aumont *et al.* (Planck Collaboration), Planck 2015 results. XIV. Dark energy and modified gravity, Astron. Astrophys. **594**, A14 (2016).

[100] G. F. Abellan, R. Murgia, V. Poulin, and J. Lavalle, Hints for decaying dark matter from S_8 measurements, arXiv:2008.09615.
[101] S. Heimersheim, N. Schöneberg, D. C. Hooper, and J. Lesgourgues, Cannibalism hinders growth: Cannibal Dark Matter and the S_8 tension, J. Cosmol. Astropart. Phys. 12 (2020) 016.
[102] R. A. Battye and A. Moss, Evidence for Massive Neutrinos from Cosmic Microwave Background and Lensing Observations, Phys. Rev. Lett. **112**, 051303 (2014).
[103] E. Di Valentino, A. Melchiorri, O. Mena, and S. Vagnozzi, Interacting dark energy in the early 2020s: A promising solution to the H_0 and cosmic shear tensions, Phys. Dark Universe **30**, 100666 (2020).
[104] E. Di Valentino *et al.*, Cosmology intertwined III: $f\sigma_8$ and S_8, Astropart. Phys. **131**, 102604 (2021).
[105] J. Lesgourgues and S. Pastor, Massive neutrinos and cosmology, Phys. Rep. **429**, 307 (2006).
[106] M. M. Ivanov, M. Simonović, and M. Zaldarriaga, Cosmological parameters and neutrino masses from the final planck and full-shape BOSS data, Phys. Rev. D **101**, 083504 (2020).
[107] C. M. Hirata, Tidal alignments as a contaminant of redshift space distortions, Mon. Not. R. Astron. Soc. **399**, 1074 (2009).
[108] S. Singh, B. Yu, and U. Seljak, Fundamental Plane of BOSS galaxies: Correlations with galaxy properties, density field and impact on RSD measurements, Mon. Not. R. Astron. Soc. **501**, 4167 (2021).
[109] A. Obuljen, W. J. Percival, and N. Dalal, Detection of anisotropic galaxy assembly bias in BOSS DR12, J. Cosmol. Astropart. Phys. 10 (2020) 058.
[110] T. Baldauf, U. Seljak, V. Desjacques, and P. McDonald, Evidence for quadratic tidal tensor bias from the halo bispectrum, Phys. Rev. D **86**, 083540 (2012).
[111] V. Desjacques, D. Jeong, and F. Schmidt, Large-scale galaxy bias, Phys. Rep. **733**, 1 (2018).
[112] A. Eggemeier, R. Scoccimarro, M. Crocce, A. Pezzotta, and A. G. Sánchez, Testing one-loop galaxy bias: Power spectrum, Phys. Rev. D **102**, 103530 (2020).
[113] T. Lazeyras, C. Wagner, T. Baldauf, and F. Schmidt, Precision measurement of the local bias of dark matter halos, J. Cosmol. Astropart. Phys. 02 (2016) 018.
[114] T. Lazeyras and F. Schmidt, Beyond LIMD bias: a measurement of the complete set of third-order halo bias parameters, J. Cosmol. Astropart. Phys. 09 (2018) 008.
[115] M. M. Abidi and T. Baldauf, Cubic halo bias in Eulerian and Lagrangian space, J. Cosmol. Astropart. Phys. 07 (2018) 029.
[116] A. Barreira, T. Lazeyras, and F. Schmidt, Galaxy bias from forward models: linear and second-order bias of IllustrisTNG galaxies, J. Cosmol. Astropart. Phys. 08 (2021) 029.
[117] V. Yankelevich and C. Porciani, Cosmological information in the redshift-space bispectrum, Mon. Not. R. Astron. Soc. **483**, 2078 (2019).
[118] A. Chudaykin and M. M. Ivanov, Measuring neutrino masses with large-scale structure: Euclid forecast with controlled theoretical error, J. Cosmol. Astropart. Phys. 11 (2019) 034.
[119] C. Hahn, F. Villaescusa-Navarro, E. Castorina, and R. Scoccimarro, Constraining M_ν with the bispectrum. Part I. Breaking parameter degeneracies, J. Cosmol. Astropart. Phys. 03 (2020) 040.
[120] M. M. Ivanov, Cosmological constraints from the power spectrum of eBOSS emission line galaxies, Phys. Rev. D **104**, 103514 (2021).
[121] A. Chudaykin, M. M. Ivanov, and M. Simonović, Optimizing large-scale structure data analysis with the theoretical error likelihood, Phys. Rev. D **103**, 043525 (2021).
[122] M. Schmittfull, M. Simonović, M. M. Ivanov, O. H. E. Philcox, and M. Zaldarriaga, Modeling galaxies in redshift space at the field level, J. Cosmol. Astropart. Phys. 05 (2021) 059.
[123] V. Poulin, T. L. Smith, T. Karwal, and M. Kamionkowski, Early Dark Energy can Resolve the Hubble Tension, Phys. Rev. Lett. **122**, 221301 (2019).
[124] V. Desjacques and U. Seljak, Primordial non-Gaussianity from the large-scale structure, Classical Quantum Gravity **27**, 124011 (2010).
[125] E. Sefusatti, 1-loop perturbative corrections to the matter and galaxy bispectrum with non-Gaussian initial conditions, Phys. Rev. D **80**, 123002 (2009).
[126] M. Liguori, E. Sefusatti, J. R. Fergusson, and E. P. S. Shellard, Primordial non-Gaussianity and bispectrum measurements in the cosmic microwave background and large-scale structure, Adv. Astron. **2010**, 980523 (2010).
[127] A. M. Dizgah, M. Biagetti, E. Sefusatti, V. Desjacques, and J. Noreña, Primordial non-Gaussianity from biased tracers: Likelihood analysis of real-space power spectrum and bispectrum, J. Cosmol. Astropart. Phys. 05 (2021) 015.
[128] G. Cabass, M. M. Ivanov, O. H. E. Philcox, M. Simonović, and M. Zaldarriaga, Constraints on single-field inflation from the BOSS galaxy survey, arXiv:2201.07238.
[129] P. Gagrani and L. Samushia, Information content of the angular multipoles of redshift-space galaxy bispectrum, Mon. Not. R. Astron. Soc. **467**, 928 (2017).
[130] D. Regan, An inventory of bispectrum estimators for redshift space distortions, J. Cosmol. Astropart. Phys. 12 (2017) 020.
[131] D. Gualdi and L. Verde, Galaxy redshift-space bispectrum: the importance of being anisotropic, J. Cosmol. Astropart. Phys. 06 (2020) 041.
[132] T. Baldauf, M. Mirbabayi, M. Simonović, and M. Zaldarriaga, LSS constraints with controlled theoretical uncertainties, arXiv:1602.00674.
[133] N. Hand, U. Seljak, F. Beutler, and Z. Vlah, Extending the modeling of the anisotropic galaxy power spectrum to $k = 0.4h$ Mpc^{-1}, J. Cosmol. Astropart. Phys. 10 (2017) 009.
[134] B. A. Reid and D. N. Spergel, Constraining the luminous red galaxy halo occupation distribution using counts-in-cylinders, Astrophys. J. **698**, 143 (2009).
[135] C. Hikage and K. Yamamoto, Impacts of satellite galaxies on the redshift-space distortions, J. Cosmol. Astropart. Phys. 08 (2013) 019.

[136] D. Gualdi, H. Gil-Marín, M. Manera, B. Joachimi, and O. Lahav, Geometrical compression: A new method to enhance the BOSS galaxy bispectrum monopole constraints, Mon. Not. R. Astron. Soc. **484**, L29 (2019).

[137] D. Gualdi, M. Manera, B. Joachimi, and O. Lahav, Maximal compression of the redshift-space galaxy power spectrum and bispectrum, Mon. Not. R. Astron. Soc. **476**, 4045 (2018).

[138] www.sdss3.org.